A large-stroke shape memory alloy spring actuator using double-coil configuration

2015 Smart Mater. Struct. 24 095014

(http://iopscience.iop.org/0964-1726/24/9/095014)

IOP Publishing

Smart Materials and Structures

Smart Mater. Struct. 24 (2015) 095014 (21pp)

doi:10.1088/0964-1726/24/9/095014

A large-stroke shape memory alloy spring actuator using double-coil configuration

Seung-Won Kim[1], Jong-Gu Lee[2], Sungmin An[1], Maenghyo Cho[2] and Kyu-Jin Cho[1]

[1] Biorobotics Laboratory, Department of Mechanical and Aerospace Engineering/IAMD, Seoul National University, 1 Gwanak-ro, Gwanak-gu, Seoul 151–742, Korea

[2] Smart Structures and Design Laboratory, Department of Mechanical and Aerospace Engineering/IAMD, Seoul National University, 1 Gwanak-ro, Gwanak-gu, Seoul 151–742, Korea

E-mail: kjcho@snu.ac.kr

Received 26 January 2015, revised 22 June 2015
Accepted for publication 23 June 2015
Published 19 August 2015

Abstract

One way to increase the range of motion of shape memory alloy (SMA) actuators is to create displacements of the SMA associated with not only the deformation from straining but also rigid-body motion from translation and rotation. Rigid-body motion allows the SMA to create larger displacements without exceeding the maximum recovery strain so that the SMA actuators can have a larger shape recovery ratio. To improve the linear actuation stroke of SMA wire actuators, a novel SMA spring actuator is proposed that employs a double-coil geometry that allows the displacement of the SMA to be mainly induced by rigid-body motion. A double-coil SMA spring actuator is fabricated by coiling an SMA wire twice so that the double coiling results in a reduction of the initial length of the double-coil SMA spring actuator. The effects of the geometric parameters on the actuation characteristic of a double-coil SMA spring actuator are verified numerically by finite element analysis and experimentally according to a parametric study of the geometric parameters. The displacement-to-force profile of the double-coil SMA spring actuator is nonlinear, and the spring stiffness changes when the actuator transforms its configuration from a double-coil shape to a single-coil shape. According to the results of the parametric study, increasing the wire diameter increases both primary and secondary coil stiffness, and increasing the primary inner coil diameter decreases both primary and secondary coil stiffness, whereas increasing the secondary inner coil diameter decreases only the secondary coil stiffness. The result shows that one of the double-coil SMA spring actuators with an initial length of 8 mm has a recovery ratio of 1250%, while the recovery ratio of the single-coil SMA spring actuator with the same geometric parameters is 432%.

Keywords: shape memory alloy (SMA), large actuation stroke, double coil, spring, actuator

(Some figures may appear in colour only in the online journal)

1. Introduction

A shape memory alloy (SMA) is a smart material that changes its crystal structure between the martensite phase and the austenite phase by thermomechanical loading, and exhibits a shape memory effect, a super-elasticity effect, and/or a two-way effect depending on the material composition, manufacturing processes, and working environments [1]. Furthermore, SMAs have one of the highest energy densities in actuators, with more than 1000 J kg^{-1} [2]. Utilizing these features, SMAs have been widely used as both smart actuators and smart sensors in various mechanical systems, including aerospace engineering [3–5], biomedical engineering [6–9], and robotics [10–14].

However, SMAs have a maximum recoverable strain ranging from 2 to 10% [2, 15] which limits the use of SMA actuators for applications that require a large range of motion. One way to increase the range of motion is to create displacements associated with not only deformation from straining but also displacements associated with rigid-body

Table 1. Actuation characteristics according to the source type of displacement.

Source type of displacement	Strain	Rigid-body motion
Configuration	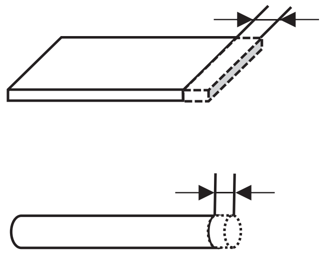	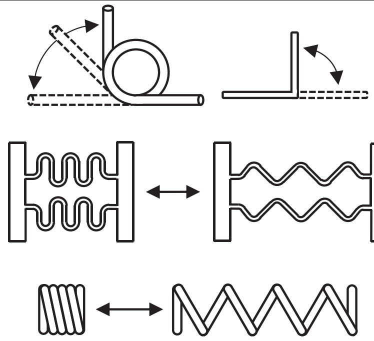
Displacement	◐○○○○	●●●●○
Force	●●●●●	●◐○○○

motion from the translation and rotation of the SMA. The rigid-body motion from translation and rotation allows for a larger range of motion of the SMA without exceeding its maximum recoverable strain, so the SMA actuator can have a larger shape recovery ratio (the shape recovery ratio is a ratio of the maximum shape recoverable displacement to the initial length of the SMA actuator). Thus, changing the geometry of the SMA has been applied to increase the range of motion for developing various types of SMA actuators. For example, sheet-type and tube-type SMA actuators have been developed by patterning geometric shapes such as zigzags, waves, or spirals [16–19]. The patterned structures of SMA actuators can produce a large range of motion by a large in-plane or out-of-plane displacement from the rigid-body motion. Such SMA actuators have an advantage in terms of having a small thickness suitable for thin spaces; however, they require a large initial length and/or area to create large actuation displacements. To increase the linear actuation stroke of an SMA actuator making use of a wire, an SMA spring actuator has been developed utilizing a coil spring configuration. As a result, the actuation stroke of the SMA spring was increased to more than 200%, although the maximum force generated by the SMA spring was decreased to less than the maximum force generated by the SMA wire [20–22]. The comparison of actuation characteristics according to the source type of displacement is listed in table 1.

Coiling is a simple and effective design method for reducing the size of wire in the length dimension, and results in a large displacement of the spring. Here, if the coiling is repeated in different ways, i.e. a single-coil spring actuator made from a wire-type actuator is coiled again, the overall length of the wire-type actuator will be reduced by much more than when the wire-type actuator is transformed into the single-coil spring actuator. Considering this, the present work focuses on a novel geometric spring—a double-coil spring—which is formed by coiling a wire twice. The wire is transformed into a single-coil spring by first coiling on a primary axis, and then the single-coil spring is transformed to a double-coil spring by the second coiling on a secondary axis. Double coiling can significantly reduce the initial length of the wire, and as a result, can increase the actuation stroke of the spring. The double-coil spring configuration has already been used for the length reduction of wires in practical applications. The tungsten filaments of an incandescent bulb use a double-coil configuration to attain high luminosity within a short length. In this case, the length of the double-coil tungsten filament is 26 times smaller than that of the tungsten filament wire, while the length of the single-coil tungsten filament is seven times smaller. Kaoua *et al* [23] and Benghanem *et al* [24] developed a model for a double-coil tungsten filament and analyzed its stress distribution. In the medical field, a double-coil configuration has been used in a surgical device for the occlusion of a large patent ductus arteriosus [25]. Furthermore, the structural configuration of chromatin in DNA forms a double-coil shape [26]. The double coil configuration in these examples indicates that the free length of the wire is reduced significantly, even though the radial size of a double-coil spring is slightly larger than that of the wire. Therefore, the geometry of a double-coil spring could help produce an extremely large recovery ratio when applied to SMA actuators.

Previous studies regarding double-coil SMA spring actuators have investigated numerical simulations based on finite element analysis (FEA) to predict the nonlinear behavior of double-coil SMA springs [27]. However, the simulation was examined under a specific deformation maintaining the spring shape as a double coil. To understand the overall behavior of a double-coil SMA spring actuator, the post-conversion of the double-coil SMA spring actuator from a double-coil shape to a single-coil shape should be verified.

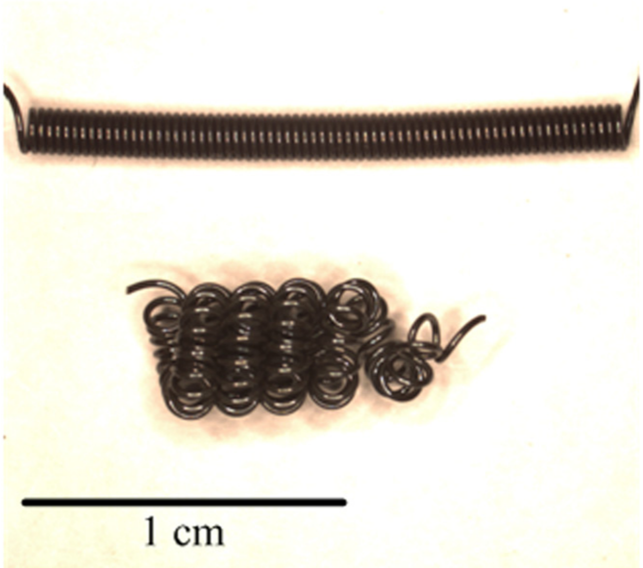

Figure 1. A single-coil SMA spring (top) and a double-coil SMA spring (bottom), with the same wire diameter, same primary coil diameter, and the same number of primary coils.

This paper presents a double-coil SMA spring actuator fabricated by coiling an SMA wire twice for a large shape recovery ratio. The investigation into the overall behaviors of the double-coil SMA spring actuator included two factors: (1) calculating the reduction of an initial length of the double-coil SMA spring actuator and the increased shape recovery ratio; and (2) verifying the effects of the geometric parameters on the actuation characteristic of the double-coil SMA spring actuator.

The rest of this paper is organized as follows: In section 2 the double-coil SMA spring actuator and its geometric parameters are introduced, and the reduction of the initial length is calculated for obtaining the shape recovery ratio. Then, a parametric study based on geometric parameters is conducted to verify their effects on the actuation characteristic. The manufacturing method of the double-coil SMA spring, the experimental setup, and the modeling of the numerical simulation are described in section 3. In section 4 the parametric study is analyzed and the experimental results and numerical simulation results are compared using FEA. A summary of the results and the conclusion are given in section 5.

2. Geometric parameters of double-coil SMA spring

The initial length of the double-coil SMA spring is shorter than that of the single-coil SMA spring due to secondary coiling, as shown in figure 1. To see how the shape recovery ratio of the double-coil SMA spring increases compared to that of the single-coil SMA spring, the initial length of both the single- and double-coil SMA springs needs to be known. Figure 2 shows the geometric parameters of the single- and double-coil springs. The geometric parameters of a typical single-coil spring are the wire diameter, d; the primary inner coil diameter, D_1; the primary pitch angle, α_1; and the number of primary coils, n_1. In the case of double-coil springs, there are additional parameters: the secondary inner coil diameter, D_2; the pitch angle of the secondary coil, α_2; and the number of secondary coils, n_2.

The initial length of the single-coil spring, L_1, is defined as

$$L_1 = n_1 \pi \left(D_1 + d\right) \tan\left(\alpha_1 + d\right). \tag{1}$$

To define the initial length of the double-coil spring, L_2, the relationship between n_1 and n_2 should be considered. If the primary coils of the double-coil spring are wound tightly so that the coils are very close together, and if $D_2 \gg d$, the number of primary coils per secondary coil, n_1^*, has a maximum value determined by the geometric relationship as

$$n_1^* = \left\lfloor \frac{\pi}{\sin^{-1}\left(\dfrac{d}{D_2 + d}\right)} \right\rfloor \approx \left\lfloor \frac{\pi\left(D_2 + d\right)}{d} \right\rfloor \tag{2}$$

where $\lfloor\rfloor$ is the floor function.

Then, n_2 is n_1 divided by n_1^*, as shown in (3), and L_2 is defined as shown in (4)

$$n_2 = \frac{n_1}{n_1^*} \tag{3}$$

$$\begin{aligned} L_2 &= n_2 \pi \left(D_2 + D_1 + 2d\right) \tan \alpha_2 + \left(D_1 + 2d\right) \\ &= \frac{n_1 d \left(D_2 + D_1 + 2d\right) \tan \alpha_2}{\left(D_2 + d\right)} + \left(D_1 + 2d\right). \end{aligned} \tag{4}$$

By dividing (1) by (4), the reduction ratio of the initial length of the double-coil spring to that of the single-coil spring, R can be expressed as

$$R = \frac{L_1}{L_2} = \frac{n_1 \pi \left(D_1 + d\right)\left(D_2 + d\right) \tan \alpha_1 + d\left(D_2 + d\right)}{n_1 d\left(D_2 + D_1 + 2d\right) \tan \alpha_2 + \left(D_1 + 2d\right)\left(D_2 + d\right)}. \tag{5}$$

For example, the theoretical length of a single-coil spring with $d = 0.25$ mm, $D_1 = 1$ mm, $\alpha_1 = 3.4°$, and $n_1 = 70$ coils is 16.58 mm, and its measured length is 18.5 mm. The theoretical length of a double-coil spring with $d = 0.25$ mm, $D_1 = 1$ mm, $D_2 = 1.18$ mm, $\alpha_2 = 9.98°$, and $n_1 = 70$ coils is 7.27 mm, and its measured length is 8 mm. In this case, the reduction ratio is 2.28 in theory and 2.31 in practice.

In addition to the reduction of the initial length, the double-coil configuration affects the actuation characteristic of the SMA spring. Generally, a single-coil SMA spring shows a linear stiffness curve when the spring stretches at the austenite phase, similar to that shown in figure 3(a). However, stretching a double-coil SMA spring transforms its geometric configuration from the secondary coil to the primary coil. In this circumstance, it is expected that the stiffness changes from a secondary coil-dominant region to a primary coil-

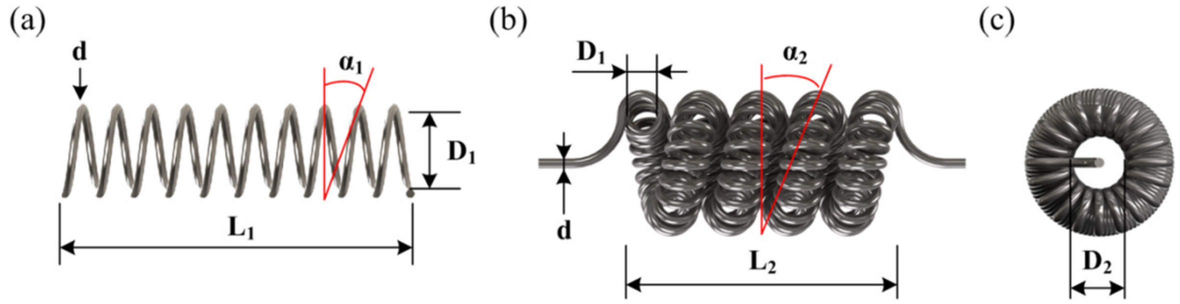

Figure 2. Geometric parameters of single- and double-coil springs: (a) lateral view of the single-coil spring, and (b) lateral view and (c) frontal view of the double-coil spring. d is the wire diameter, D_1 is the primary inner coil diameter, D_2 is the secondary inner coil diameter, α_1 is the pitch angle of the primary coil, α_2 is the pitch angle of the secondary coil, L_1 is the initial length of the single coil, and L_2 is the initial length of the double coil.

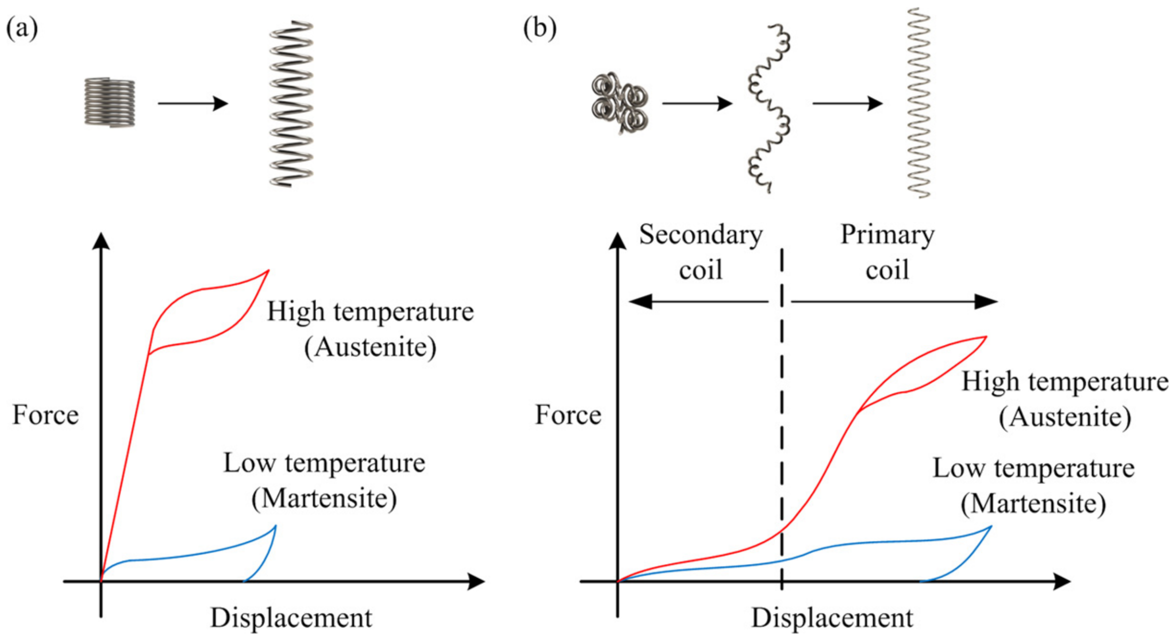

Figure 3. Typical force–displacement curve of an SMA spring: (a) single-coil SMA spring and (b) double-coil SMA spring. The left side of the dash line in (b) is for the secondary coil-dominant region and the right side is for the primary coil-dominant region.

dominant region according to the geometric change, similar to that shown in figure 3(b), but it is not yet known how and when it changes. Thus, the actuation characteristics of the double-coil SMA spring actuator are investigated.

The double-coil SMA spring actuator has many geometric parameters, with each parameter having an influence on the actuation characteristic. To verify the effect of the geometric parameters on the actuation characteristic of the double-coil SMA spring, a parametric study is performed with four test groups as follows:

- Group 1: effect of secondary coiling—secondary coiling is the main difference between single- and double-coil springs in terms of the structure; thus, the actuation characteristic will be quite different. To verify the effect of secondary coiling, a single-SMA spring and a double-coil SMA spring with the same wire diameter, primary inner coil diameter, and number of primary coils were compared.
- Group 2: effect of wire diameter—wire diameter is a fundamental geometric parameter that affects the stiffness of the spring. To verify the effect of the wire diameter, two double-coil SMA springs with different wire diameters but with the same primary inner coil diameter, secondary inner coil diameter, number of primary coils, and number of secondary coils were compared.

  Increasing the wire diameter while maintaining the secondary coil diameter decreases the number of primary coils per secondary coil, n_1^*, according to (2). For example, two double-coil springs can have the same primary inner coil diameter and the same secondary inner coil diameter but different wire diameters. If the number of primary coils is the same in both springs, the spring with a smaller wire diameter will have fewer secondary coils than the spring with a larger wire diameter. However, if the number of secondary coils is the same in both springs, the spring with a smaller wire diameter will have more primary coils than the spring with a larger wire diameter. This means that two double-coil springs with different wire diameters cannot have the same number of primary coils and the same number of secondary coils at the same time. As a result, the stiffness of the double-coil SMA spring would be affected by not only the wire diameter, but also by the number of primary or secondary coils.

To solve this problem, the number of primary coils or secondary coils should be reduced. Therefore, in the simulation two double-coil SMA springs with the same geometric parameters except for the wire diameter were compared. The number of primary coils of the double-coil SMA spring with a smaller wire diameter was reduced to that of the double-coil SMA spring with a larger wire diameter. In this case, decreasing the number of primary coils of the double-coil SMA spring with a smaller wire diameter increases the pitch angle of the primary coil, but the increased pitch angle does not affect the stiffness of the spring.

In the experiment, however, two double-coil SMA springs with different wire diameters were used, which have maximum n_1^* because adjusting n_1^* during manufacturing was difficult. Thus, the double-coil SMA spring with a smaller wire diameter had more primary coils in the experiment than the double-coil SMA spring in the simulation. Therefore, verifying the effect of wire diameter was mainly achieved by comparing the results of the two springs in the simulation, and the experimental results were used to support the simulation results.

- Group 3: effect of the primary inner coil diameter—to verify the effect of the primary inner coil diameter, two double-coil SMA springs with different primary inner coil diameters but with the same wire diameter, secondary inner coil diameter, number of primary coils, and number of secondary coils were compared.
- Group 4: effect of the secondary inner coil diameter—to verify the effect of the secondary inner coil diameter, two double-coil SMA springs with different secondary inner coil diameters but with the same wire diameter, primary inner coil diameter, number of primary coils, and number of secondary coils were compared.

According to (4), changing the secondary inner coil diameter affects the number of primary coils per secondary coil as well. To solve this problem, an approach similar to that used for Group 2 was used for this group. In the simulation, two double-coil SMA springs with the same geometric parameters except for the secondary inner coil diameter were used. In this case, the number of primary coils of the double-coil SMA spring with a large secondary inner coil diameter was reduced to that of a double-coil SMA spring with a small secondary inner coil diameter.

In the experiment, two double-coil SMA springs with the same diameters except for the secondary inner coil diameter were used, and each of them had maximum n_1^* according to (2). Therefore, the double-coil SMA spring with a larger secondary inner coil diameter had a larger number of primary coils in the experiment than the double-coil SMA spring with a smaller secondary inner coil diameter in the simulation. Verifying the effect of the secondary inner coil diameter was mainly achieved by comparing the results of the two springs in the simulation, and the experimental results were used to support the simulation results.

According to this parametric study, a numerical simulation based on the finite element method and an experiment with a tensile loading test were performed.

3. Methods

3.1. Manufacturing

The manufacturing process of the double-coil SMA spring actuator is similar to that of typical coil springs. First, an SMA wire (Dynalloy, Inc.) was tightly wound around a rod with diameter D_1 using a hand-drill device to form the primary coil shape (figure 4(a)), which was then fixed by clamping both ends of the SMA wire with bolts, nuts, and washers (figure 4(b)). This wound wire was put into a furnace to memorize the single-coil shape using heat annealing. After the first heat annealing, a single-coil SMA spring was produced (figure 4(c)). Next, this single-coil spring was wound around another rod with diameter D_2 to form the double-coil shape (figure 4(d)). In this process, maintaining a uniform number of primary coils per secondary coil, n_1^*, is important, but this is very difficult because of the complexity of the hierarchical configuration of the double-coil spring. To maintain n_1^* uniformly, the appropriate tension was carefully applied by hand to the single-coil SMA spring actuator during winding so that it could be wound without irregular stretching and distortion. The wound single-coil SMA spring was fixed by clamping both ends with bolts, nuts, and washers (figure 4(e)), and was again treated by heat annealing. Finally, the double-coil SMA spring was produced, as shown in figure 4(f). All of the SMA springs were subjected to the same annealing procedure of 400 °C for 1 h to ensure the consistency of the thermo-mechanical characteristics of the SMA springs. In addition, all of the SMA springs were manufactured with a minimum pitch during winding, which means that each primary coil and secondary coil are in contact with other primary and secondary coils, respectively (see figures 4(a) and (d)). The three diameters of the double-coil SMA spring actuator used in the experiment are listed in table 2.

For convenience of notation, the designed SMA springs are represented by arranging the constitutive diameters in order. For example, if a single-coil SMA spring has a 0.25 mm wire diameter and a 1 mm primary inner coil diameter, the notation is 0.25-1. Similarly, if a double-coil SMA spring has a 0.25 mm wire diameter, a 1 mm primary inner coil diameter, and a 3 mm secondary inner coil diameter, the notation is 0.25-1-3. Using this notation, the four groups in the parametric study used the categorized springs as follows:

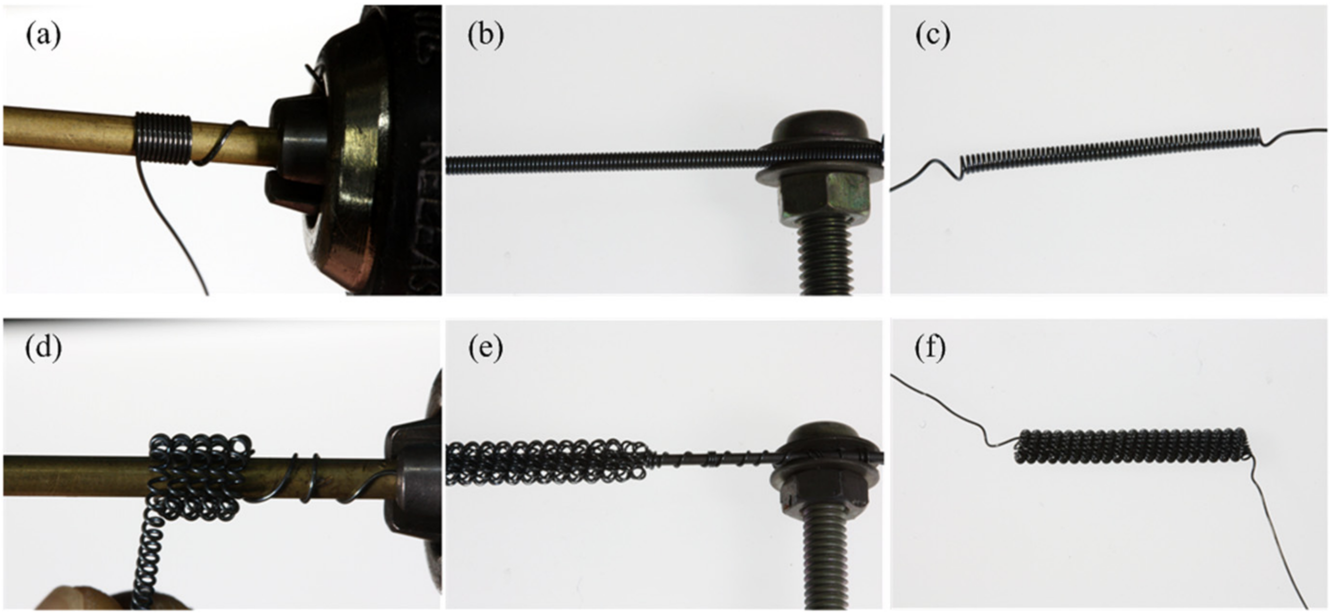

Figure 4. Manufacturing process of the double-coil SMA spring actuator.

Table 2. Diameters of double-coil SMA spring actuator.

Quantity	Unit	Value
Wire diameter, d		0.25, 0.3
Primary coil diameter, D_1	mm	0.5, 1
Secondary coil diameter, D_2		1, 3

- Group 1 to determine the effect of secondary coiling: 0.25-1 and 0.25-1-1
- Group 2 to determine the effect of wire diameter: 0.25-1-1 and 0.3-1-1
- Group 3 to determine the effect of primary coil diameter: 0.25-0.5-1 and 0.25-1-1
- Group 4 to determine the effect of secondary coil diameter: 0.3-1-1 and 0.3-1-3

However, there was an issue with the production of the double-coil SMA spring actuator: the manufactured double-coil SMA spring actuators had a slightly larger secondary inner coil diameter than the originally designed secondary inner coil diameter with D_2. This problem can be caused by various factors, but the major factor is the rearrangement of the crystal structure in the SMA due to a low pretension for secondary coiling. As mentioned previously, in order to prevent the double-coil spring from experiencing irregular stretching and distortion while undergoing secondary coiling, it was not possible to apply high pretension to the double-coil SMA spring. Owing to the low pre-tension, a gap exists between the primary coils, and this induced a rearrangement of the crystal structure of the SMA when undergoing heat annealing. As a result, the fixed shape of the secondary coil was released after unclamping, and the secondary coil diameter increased, which is similar to the spring back effect from typical metal bending processes. The increased secondary inner coil diameter could not be predicted, but the number of primary coils per secondary coil of the actual double-coil SMA spring actuators is the same as the number of primary coils per secondary coil calculated from (2). Therefore, the spring notation was still used while specifying the increased secondary coil diameter for the experimental results in section 4. This was also reflected in the simulation.

3.2. Experimental setup

3.2.1. Differential scanning calorimetry (DSC). The thermomechanical process during the manufacturing process of an SMA spring affects phase transformation temperatures, thus the phase transformation temperature should be verified. The changed transformation temperatures were measured by differential scanning calorimetry (DSC). Six test samples were prepared for the DSC test with one SMA wire as received from the manufacturer, and five SMA springs after annealing. Test samples with a weight of 20 mg were cut from the SMA wire and springs and put into a pan. The pan was put into a DSC machine (Perkin Elmer, Diamond DSC), and tested under a thermal cycle with a heat flow rate of 10 °C min^{-1} between −50 and 100 °C. For reliability of the result from the DSC, the sample was at first heated from 25 to 100 °C, and the thermal cycle was repeated twice. An example of the DSC result of the 0.25-1-1 SMA spring is shown in figure 5, and the measured transformation temperatures, averages and standard deviations are listed in table 3. A^s, A^f, R^s, R^f, M^s, and M^f are the austenite start, austenite finish, R-phase start, R-phase finish, martensite start, and martensite finish temperatures, respectively .

In figure 5, the upper curve is for heating and the lower curve is for cooling. The upper peak is due to the endothermic latent heats of transformation at the austenite phase and the lower two peaks are due to the exothermic latent heats of transformation at the R-phase and martensite phase. From the right to left in the lower curve, the first peak is for the R-phase

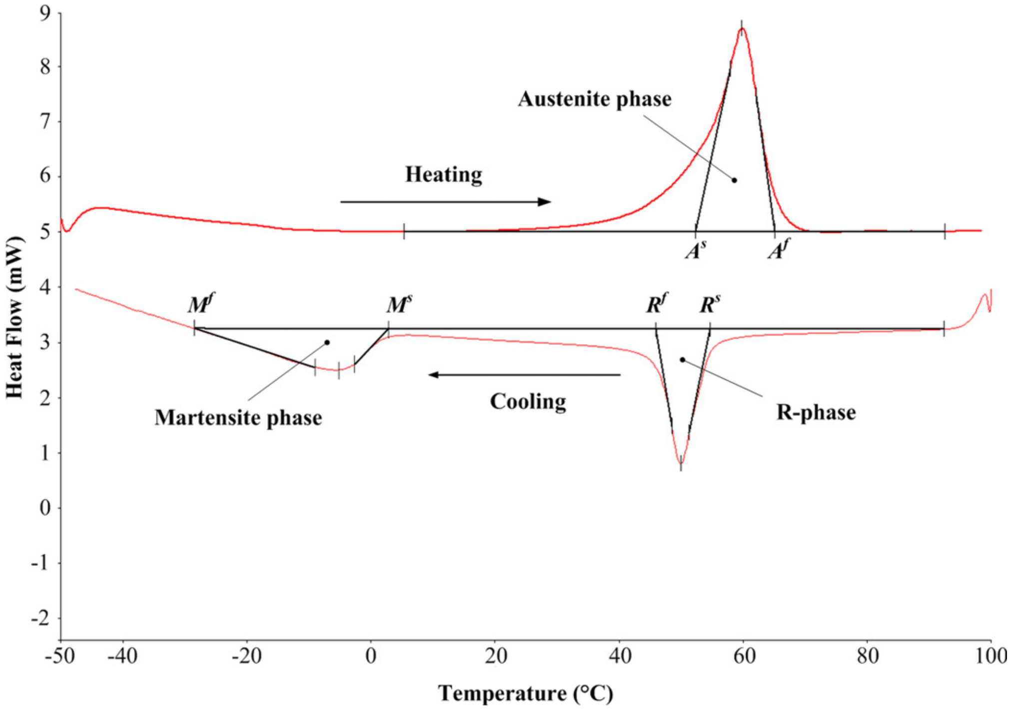

Figure 5. DSC result of the 0.25-1-1 SMA spring.

Table 3. Measured transformation temperatures of the SMA actuators.

Transformation temperature	(a)	(b)	(c)	(d)	(e)	(f)	[a]Average	[a]Standard deviation
A^s (°C)	59.0	52.0	50.8	52.3	52.6	52.4	52.0	1.16
A^f (°C)	66.9	62.0	64	65.1	64.0	64.6	63.9	0.70
R^s (°C)	72.4	53.8	55.5	54.4	54.2	55.2	54.6	0.72
R^f (°C)	42.3	47.6	46.5	46.2	46.3	45.5	46.4	0.76
M^s (°C)	27.2	2.1	1.0	2.3	2.3	−0.3	1.5	1.14
M^f (°C)	10.6	−21.4	−35.5	−29.6	−31.3	−31.3	−29.8	5.18

[a] The average and standard deviation values are calculated from the five SMA springs from (b) to (f).
(a) SMA wire with a diameter of 0.25 mm, (b) 0.25-1 spring, (c) 0.25-0.5-1 spring, (d) 0.25-1-1 spring, (e) 0.3-1-1 spring, and (f) 0.3-1-3 spring.

and the second peak is for the martensite phase. In the exothermic or endothermic curves, the start and finish temperature of transformation can be determined at the intersection of the two straight black lines, where one is the horizontal base line and the other is a straight line fitted to the steepest sides of the peak. According to the DSC result, the measured A^S and A^f are lower than A^f (70 °C) from the data sheet of the manufacturer, and the M^f is much lower than room temperature (20 °C). In particular, the standard deviation of M^f is large because the exothermic process of the martensite did not finish, and it is hard to determine precisely where the intersection is. This problem that the temperature determined by the intersection depends on the shape of the enthalpy peak and of the chosen baseline was mentioned previously in reference [28] and causes uncertainty in the result. For that reason, there is a discrepancy between the experimental and simulation results. This will be discussed in further detail later.

3.2.2. Tensile test of SMA springs. The experimental setup for tensile testing of the SMA springs is shown in figure 6. The tensile testing machine (RB302 ML, R&D Inc. Korea) has a heat chamber with a hole to allow a tension rod to move into the heat chamber (see figure 6(a)). Both ends of each specimen of SMA spring were clamped using ring terminals, which were hung on the hooks of the tensile rod (see figure 6(b)).

The test was conducted at two temperatures, the first being room temperature (20 °C) where the SMA spring is in the full twinned martensite state, and the other at a high temperature (200 °C) where the SMA spring is in the full austenite state. Before the tensile test, all specimens are cooled down to below the martensite finish temperature using an instant freezing aerosol spray (NABAKEM, SF-1013 NPP) which can cool the surface temperature of materials to −50 °C. The diameter of the SMA wire is small enough to allow the spray to transform the crystal phase of the SMA

Table 4. Material constants of SMA wire.

Parameter	Specification	Unit	Value	Note
E^M	Young's modulus of martensite	GPa	21.07	Estimated
E^A	Young's modulus of austenite	GPa	54.796	Estimated
ν^M	Poisson's ratio of martensite	—	0.33	[a]From data sheet
ν^A	Poisson's ratio of austenite	—	0.33	[a]From data sheet
α^M	Thermal expansion coefficient of martensite	1/K	6.6×10^{-6}	[a]From data sheet
α^A	Thermal expansion coefficient of austenite	1/K	11.0×10^{-6}	[a]From data sheet
H	Maximum transformation strain	—	0.0288	Measured
ρ	Mass density	kg m^{-3}	6450	[a]From data sheet
A^s	Austenite start temperature	K	325.2	Measured
A^f	Austenite finish temperature	K	337.1	Measured
M^s	Martensite start temperature	K	274.7	Measured
M^f	Martensite finish temperature	K	243.4	Measured
Δc	Difference of specific heat between martensite and austenite	—	0	From [29]
Δu	Difference of specific internal energy between martensite and austenite	J kg^{-1}	−10 474	Estimated
Δs	Difference of specific entropy between martensite and austenite	J kg$^{-1}\cdot$K^{-1}	−34.26	Estimated
b^A	Isotopic hardening moduli for forward transformation	J kg^{-1}	407.73	Estimated
b^M	Isotopic hardening moduli for reverse transformation	J kg^{-1}	107.24	Estimated
Y^*	Threshold of thermodynamic force Π at onset of phase transformation	MPa	7.967	Estimated

[a] Data sheet is from Dynalloy, Inc.

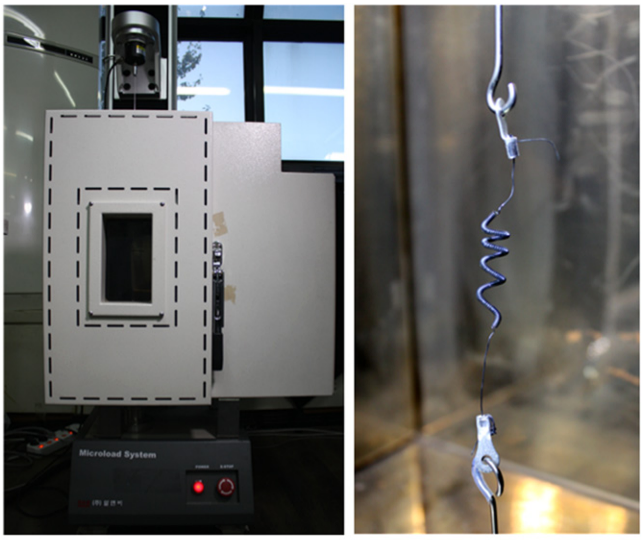

(a) (b)

Figure 6. Experimental setup: (a) tensile testing machine with a heat chamber and (b) double-coil SMA spring specimen.

springs into the full twinned martensite state. The specimen was placed in the heat chamber and enough time was allowed for the specimen to reach thermal equilibrium. The test cycle was made up of two steps: first, the SMA spring was pulled until the displacement reached a setting position, then it was released until the measured load was zero. When the test was finished, the specimen was taken out from the heat chamber, and it was then heated using a heat gun to above the austenite finish temperature to recover its shape. In the tensile test of each SMA spring, three samples were tested for reliability, and from the results the average and standard deviation of the stiffness of the SMA springs were calculated and are listed in tables in section 4. The loading and unloading speeds were 0.5 mm s^{-1}, and the data collecting rate was 10 points/s.

3.3. Numerical simulation using the finite element method

FEA was performed to predict the behavior of the single- and double-coil SMA springs. First, FE models of both springs were discretized by 8-node isoparametric quadrilateral elements, and the cross section of the FE model consisted of 16 elements, as shown in figure 7(a). The cross sections faced each other at regular intervals along the trajectory of the single- and double-coil spring (i.e. the center axis of the SMA wire, as shown in figure 7(b)). The trajectories of the single-coil, φ_t^s, and double-coil spring, φ_t^d, were expressed in a Cartesian coordinate system by (6) and (7), respectively. In the FEA simulation, the measured geometric parameters of the manufactured double-coil SMA springs were used. The number of assembled elements in the FE model was approximately 32 000.

$$\vec{\varphi}_t^{\,s} = \vec{\varphi}_t^{\,s}(x(t),\quad y(t),\quad z(t)),$$

where

$$\begin{bmatrix} x(t) = \dfrac{D_1+d}{2}\cos\left(\dfrac{D_1+d}{2n_1}t\right) \\ y(t) = \dfrac{D_1+d}{2}\sin\left(\dfrac{D_1+d}{2n_1}t\right) \\ z(t) = \dfrac{d\left(D_1+d\right)}{4n_1\pi}t \end{bmatrix} \tag{6}$$

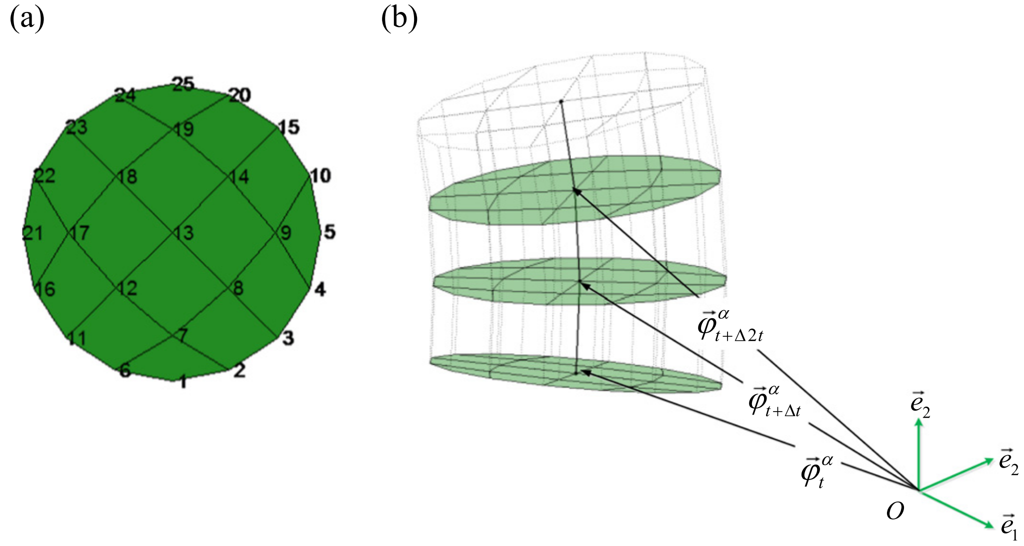

Figure 7. FE model of SMA wire. (a) Cross section of SMA wire and (b) its arrangement along the center axis of the SMA wire.

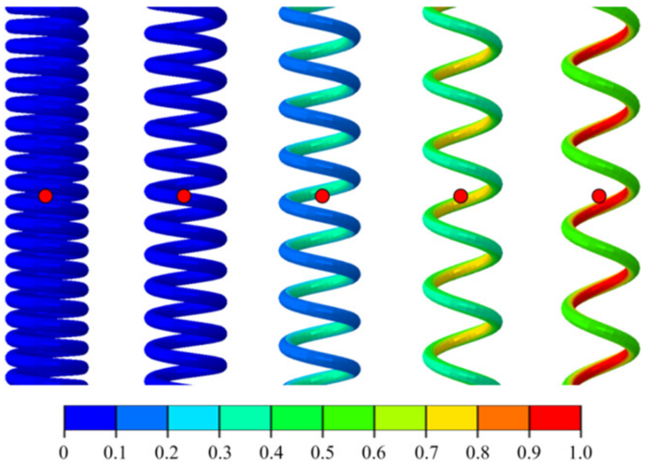

Figure 8. Distribution of detwinned martensite volume fraction in the FEA model of the 0.25-1 spring at 20 °C. The red dot is a reference point.

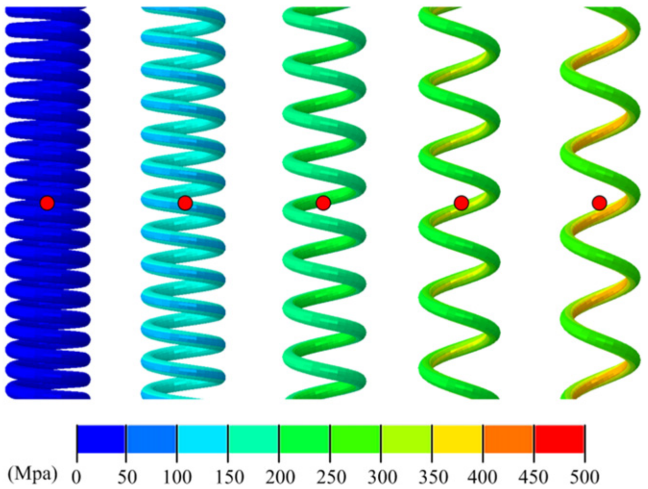

Figure 9. Distribution of the von Mises stress in the FEA model of the 0.25-1 spring at 20 °C. The red dot is a reference point.

$$\vec{\varphi}_t^{d} = \vec{\varphi}_t^{d}\Big(x^*(t),\quad y^*(t),\quad z^*(t)\Big),\qquad \text{where}$$

$$\begin{bmatrix} x^*(t) = \cos\left(\dfrac{D_1 + d}{2n_1^*}t\right) \\ \qquad \times\left[\dfrac{D_1 + D_2 + 2d}{2} + \dfrac{D_1 + d}{2}\cos\left(\dfrac{D_1 + d}{2}t\right)\right] \\ y^*(t) = \sin\left(\dfrac{D_1 + d}{2n_1^*}t\right) \\ \qquad \times\left[\dfrac{D_1 + D_2 + 2d}{2} + \dfrac{D_1 + d}{2}\cos\left(\dfrac{D_1 + d}{2}t\right)\right] \\ z^*(t) = \left[\dfrac{(D_1 + 2d)(D_1 + d)}{4n_1^*\pi}\right]t \\ \qquad + \dfrac{D_1 + d}{2}\sin\left(\dfrac{D_1 + d}{2}t\right) \end{bmatrix} \tag{7}$$

To reflect the behavior of the SMA in FEA, the Lagoudas model, which is a three-dimensional (3D) SMA model, was implemented in ABAQUS, a commercial FEA package [29]. Initially, a transformation function Φ had to be defined because the transformation function specifies the criteria of the phase transformation of the SMA. The transformation function was divided into two criteria with respect to the forward and reverse transformations as follows:

$$\Phi = \begin{cases} \Pi^f - Y^* > 0, & \dot{\xi}_s > 0: \ \text{forward transformation} \\ -\Pi^b - Y^* < 0, & \dot{\xi}_s < 0: \ \text{reverse transformation} \end{cases} \tag{8}$$

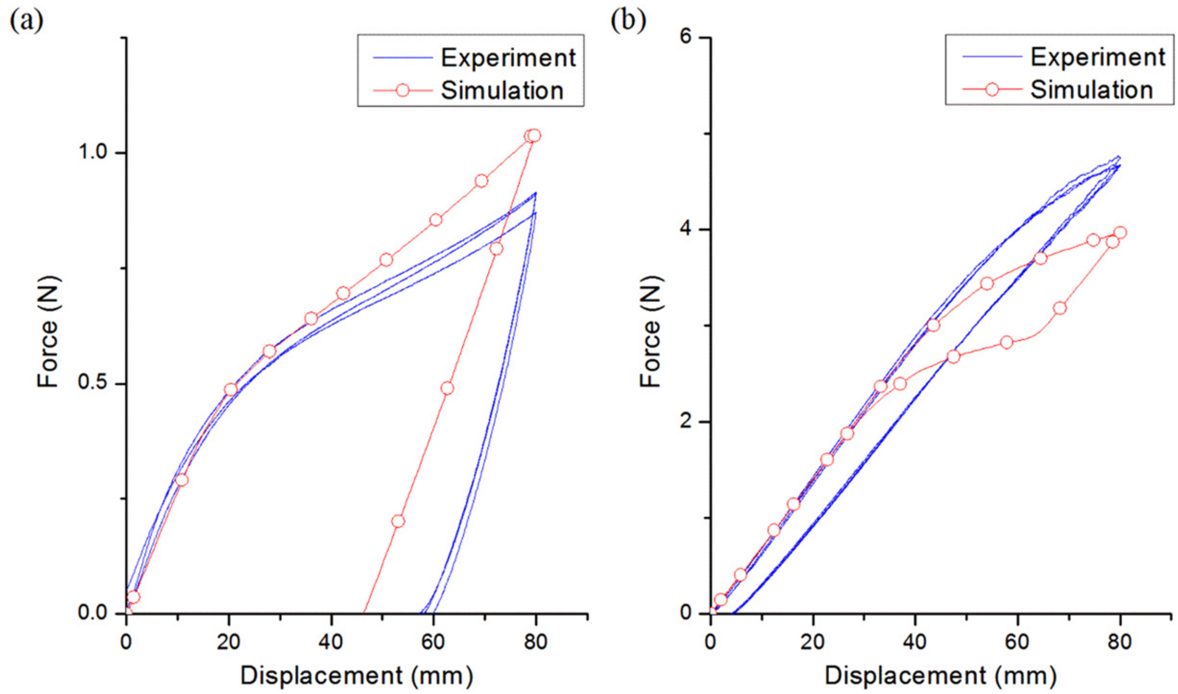

Figure 10. Comparison between the FE simulation and experiment of the 0.25-1 spring with 72 coils: (a) at 20 °C and (b) at 200 °C.

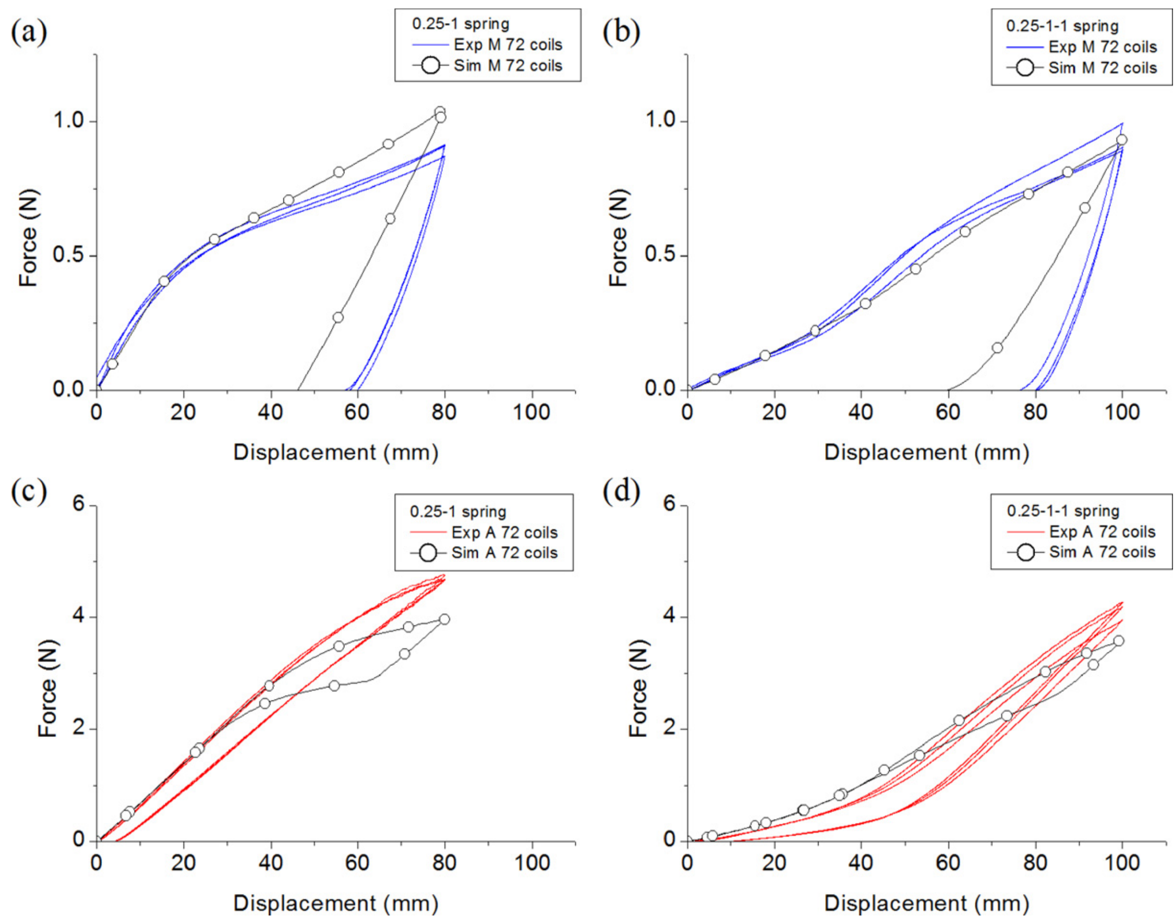

Figure 11. Displacement-to-force graphs of single- and double-coil SMA springs: (a) 0.25-1 single-coil spring at 20 °C, (b) 0.25-1-1 spring at 20 °C, (c) 0.25-1 single-coil spring at 200 °C, and (d) 0.25-1-1 double-coil spring at 200 °C. Sim—simulation, Exp—experiment, M—martensite phase at 20 °C, and A—austenite phase at 200 °C. The coil number is the number of primary coils.

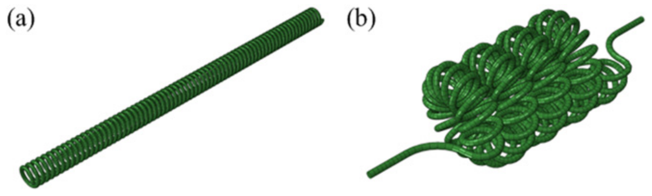

Figure 12. Simulation model of (a) 0.25-1 spring with 72 coils and (b) 0.25-1-1 spring with 72 coils.

where

$$\begin{cases} \Pi^f &= \sigma_{ij}\Lambda_{ij} + \frac{1}{2}\Delta S_{ijkl}\sigma_{ij}\sigma_{kl} + \Delta\alpha_{ij}\sigma_{ij}\Delta T \\ & \quad + \rho\left[\Delta c\left(\Delta T - T\ln\frac{T}{T_0}\right) + \Delta s_0 T \right.\\ & \quad \left. - \Delta u_0 - b^M\xi_s - \left(\mu_1 + \mu_2\right)\right] \\ &\cong Y^* \\ \Pi^b &= \sigma_{ij}\Lambda_{ij} + \frac{1}{2}\Delta S_{ijkl}\sigma_{ij}\sigma_{kl} + \Delta\alpha_{ij}\sigma_{ij}\Delta T \\ & \quad + \rho\left[\Delta c\left(\Delta T - T\ln\frac{T}{T_0}\right) + \Delta s_0 T \right.\\ & \quad \left. - \Delta u_0 - b^A\xi_s - (\mu_1 - \mu_2)\right] \\ &\cong -Y^* \end{cases} \quad (9)$$

where

$$\Delta S_{ijkl} = S_{ijkl}^M - S_{ijkl}^A$$
$$\Delta\alpha_{ij} = \alpha_{ij}^M - \alpha_{ij}^A$$
$$\Delta c = c^M - c^A$$
$$\Delta s_0 = s_0^M - s_0^A$$
$$\Delta u_0 = u_0^M - u_0^A. \quad (10)$$

The forward transformation is a phase transformation from the parent phase (twinned martensite or austenite phase) to the detwinned martensite phase, and the reverse transformation is a phase transformation from the detwinned martensite phase to the austenite phase. The variables σ_{ij}, Λ_{ij}, S_{ijkl}^{λ}, and α_{ij}^{λ} are the stress tensor, transformation tensor, elastic compliance tensor, and thermal expansion tensor, respectively. The superscript λ denotes the reference state of the phase (i.e. M is for the martensite state and A is for the austenite state). Additionally, T, ρ, s_0, c, u_0, and ξ_s are the temperature, mass density, specific entropy, specific heat, specific internal energy, and detwinned martensite volume fraction, respectively. The detwinned martensite volume fraction, ξ_s, is distinguished from the twinned martensite volume fraction, ξ_t. The total martensite volume fraction, ξ, is defined by sum of the detwinned and twinned martensite volume fractions (i.e. $\xi = \xi_s + \xi_t$). The variables b^{λ}, μ_1, and μ_2 are hardening parameters. Among the hardening parameters, parameters b^A and b^M represent the isotropic hardening moduli for the forward and reverse transformations respectively, and the parameter μ_2 is determined from the continuity condition of the polynomial-form hardening function [29]. Although parameter μ_1 physically denotes the accumulation of elastic strain energy when the forward transformation begins, it is omitted for simplicity. These hardening parameters are expressed as

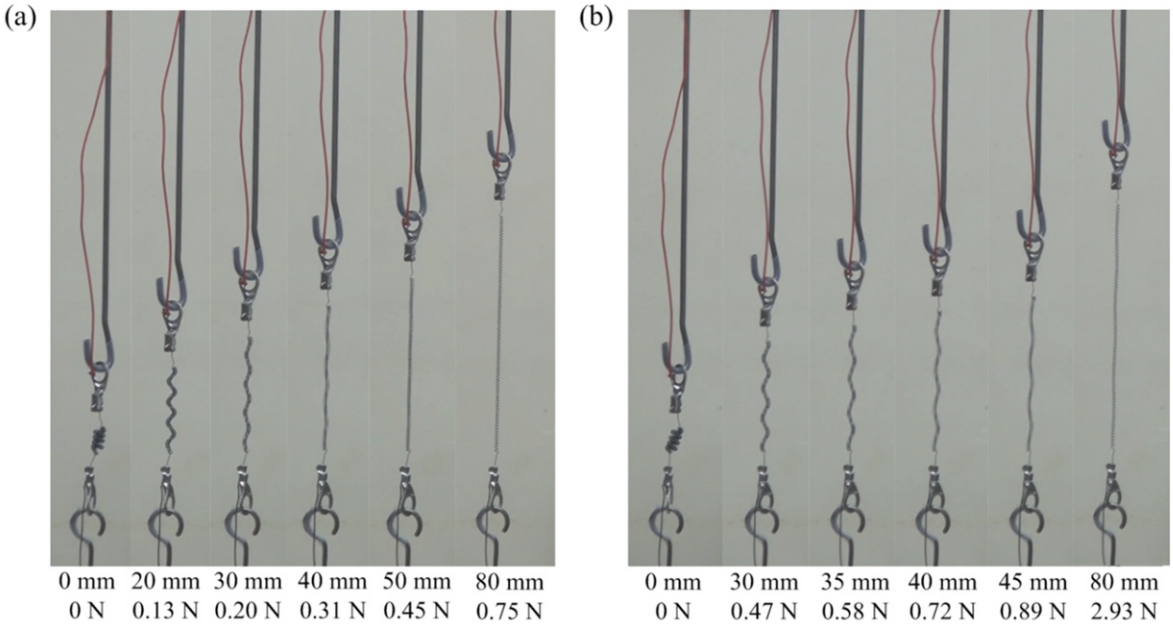

Figure 13. Snapshots of the 0.25-1-1 spring for tensile tests at (a) 20 °C in the martensite phase and (b) 200 °C in the austenite phase. The elongated length and measured force are indicated under each snapshot.

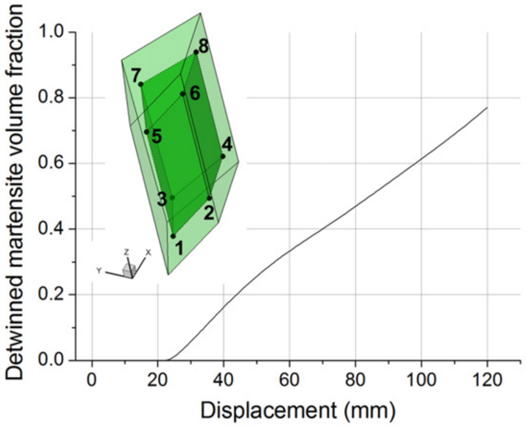

(a)

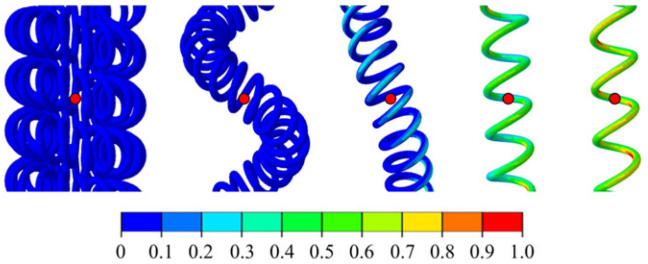

(b)

Figure 14. Detwinned martensite volume fraction in the FEA model of the 0.25-1-1 spring at 20 °C: (a) displacement to the detwinned martensite volume fraction that is an averaged value of eight Gauss points (bold numbers) inside the selected element at a reference point; (b) distribution of the detwinned martensite volume fraction. Red dot is a reference point.

follows:

$$
\begin{aligned}
b^A &= -\Delta s_0\left(A^f - A^s\right)\\
b^M &= -\Delta s_0\left(M^s - M^f\right)\\
\mu_2 &= \frac{1}{4}\rho\left(b^A - b^M\right)
\end{aligned}
\tag{11}
$$

Finally, Y^* denotes the threshold of thermodynamic force Π at the onset of phase transformation.

The role of the thermodynamics force is similar to the yield surface in the theory of plasticity. Therefore, the numerical scheme is also simply applied for the evaluation of the transformation strain. When the strain and temperature are given, the increment of the detwinned martensite volume fraction and the transformation strain and stress can be calculated using a return mapping algorithm [29]. The distributions of the detwinned martensite volume fraction and transformation stress are illustrated in figures 8 and 9, respectively.

To obtain material constants such as Young's modulus, the tensile test of the 0.25-1 spring was performed at 200 °C for the 100% austenite state and 20 °C for the 100% twinned martensite state, as can be seen in figure 10. From this tensile test, the obtained displacement-to-force curve of the single-coil SMA spring can be transformed to the shear stress–shear strain curve. To do this mapping procedure, a relation between the axial force and the final pitch angle of the single coil spring after deformation, and a relation between the shear stress and the axial force are utilized as follows [20]

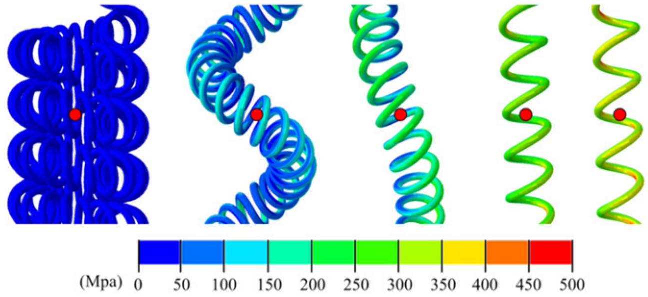

Figure 15. Distribution of the von Mises stress in the FEA model of the 0.25-1-1 spring at 20 °C. Red dot is a reference point.

$$
F = \frac{\pi d^4}{8\left(D_1 + 2d\right)^2} G \frac{\cos^2\alpha_i\left(\sin\alpha_f - \sin\alpha_i\right)}{\cos^2\alpha_f\left(\cos^2\alpha_f + \sin^2\alpha_f/(1+\nu)\right)}
\tag{12}
$$

where α_i and α_f are the initial pitch angle of the single coil spring before deformation and the final pitch angle of single coil spring after deformation respectively, which have to be estimated by deflection and the final pitch angle relation. The derivation progress of (12) is explained in further details by An *et al* [20].

$$
\tau = \frac{T(d/2)}{J} = \frac{F\left(\dfrac{D_1 + 2d}{2}\right)\left(\dfrac{d}{2}\right)}{\left(\pi d^4/32\right)} = \frac{8\left(D_1 + 2d\right)F}{\pi d^3} = \frac{8CF}{\pi d^2}
\tag{13}
$$

where J denotes the polar moment of inertia and C denotes the spring index (i.e. $C = \left(D_1 + d\right)/d$); T is the torsional moment applied to the cross-section of the single spring and F is the force applied to the axial deflection of spring.

By substituting the axial force, F, of equation (12) into the shear stress of equation (13), and then rearranging the results into a shear stress–shear strain relation form, $\tau = G\gamma(C,\ \mathrm{v},\ \alpha_i,\ \alpha_f)$, the shear strain, $\gamma(C,\ \nu,\ \alpha_i,\ \alpha_f)$ can be derived as follows:

$$
\gamma = \frac{1}{C}\frac{\cos^2\alpha_i\left(\sin\alpha_f - \sin\alpha_i\right)}{\cos^2\alpha_f\left(\cos^2\alpha_f + \sin^2\alpha_f/(1+\nu)\right)} = \frac{\tau}{G}
\tag{14}
$$

From these procedures, the transformed shear stress and shear strain curve was obtained, which is similar to the displacement-to-force curve. The transformed shear stress–shear strain curve shows a nonlinear relation due to the phase transformation of the SMA. However, below a 1% shear strain, this curve shows an almost linear relation. Therefore,

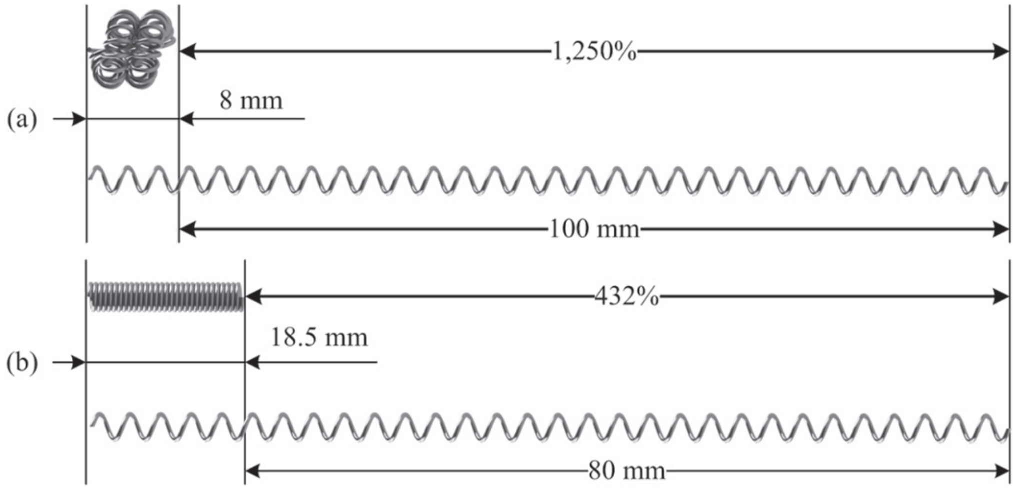

Figure 16. Comparison of shape recovery ratios between (a) 0.25-1-1 spring and (b) 0.25-1 spring.

Table 5. Stiffnesses of 0.25-1 and 0.25-1-1 SMA springs in the martensite and austenite phases. Exp—experiment, Sim—Simulation, SD—Standard deviation, Error—percentage of difference between the experiment and simulation with respect to the simulation.

		Primary coil stiffness (N mm^{-1})							
		Martensite				Austenite			
Spring type	Number of primary coils	Sim	Exp	SD	Error(%)	Sim	Exp	SD	Error(%)
0.25-1	72	0.027	0.029	0.0031	7.4	0.070	0.074	0.0004	5.7
0.25-1-1	72	0.012	0.014	0.0009	16.7	0.049	0.065	0.0024	32.7
		Secondary coil stiffness (N mm^{-1})							
		Martensite				Austenite			
Spring type	Number of primary coils	Sim	Exp	SD	Error(%)	Sim	Exp	SD	Error(%)
0.25-1	72	—	—	—	—	—	—	—	—
0.25-1-1	72	0.008	0.008	0.0003	0	0.019	0.018	0.0008	−5.3

the shear moduli G_A and G_M were easily estimated using the linear fitting of the shear stress–shear strain curve with respect to the 100% austenite state and the 100% twinned martensite state respectively, below a 1% shear strain. Furthermore, it can be considered as an isotropic material in the case of a polycrystalline material, i.e. the SMA wire in this study. So, these shear moduli can be easily converted into the Young's modulus by $2(1+\nu)G$, where ν is Poisson's ratio. A Poisson's ratio of 0.33 is used based on the data sheet from the manufacturer. The maximum transformation shear strain γ_t was defined by estimating the unrecovered shear strain after unloading at the end of the detwinning. The maximum transformation strain, H, was calculated by $\gamma_t/\sqrt{3}$, and this relation is equivalent to the effective strain of pure strain in the plasticity.

The four transformation temperatures, A^s, A^f, M^s, and M^f are obtained from DSC as explained in section 3.2.1. The difference of specific entropy between the martensite and austenite, Δs, is estimated by dividing the mean values of the exchanged heat during transformation, ΔH, by the phase equilibrium temperature, T_{eq} [30]. The phase equilibrium temperature can be approximately obtained by calculating, $T_{eq} = \frac{1}{2}M^s + A^f$ [31]. The difference of specific internal energy between martensite and austenite, Δu, can be obtained by calculating, $\Delta u = T_{eq}\Delta s$ [29]. It is assumed that there is no difference in specific heat between the martensite and austenite phase, Δc, because the specific heats are almost equal to each other (i.e. during forward transformation and reverse transformation) [29]. The isotropic hardening modulus for forward transformation, b^A, and the isotropic hardening modulus for reverse transformation, b^M, are obtained by using $b^A = \Delta s\left(A^f - A^s\right)$ and $b^M = \Delta s\left(M^s - M^f\right)$ respectively. The threshold of thermodynamic force Π at the onset of phase transformation, Y^*, is calculated by $Y^* = -\frac{1}{2}\rho\Delta s\left(A^f - M^s\right) - \frac{1}{4}\rho\Delta s\left(M^s - M^f - A^f + A^s\right)$ [29]. The material constants of SMA used in the simulation are listed in table 4.

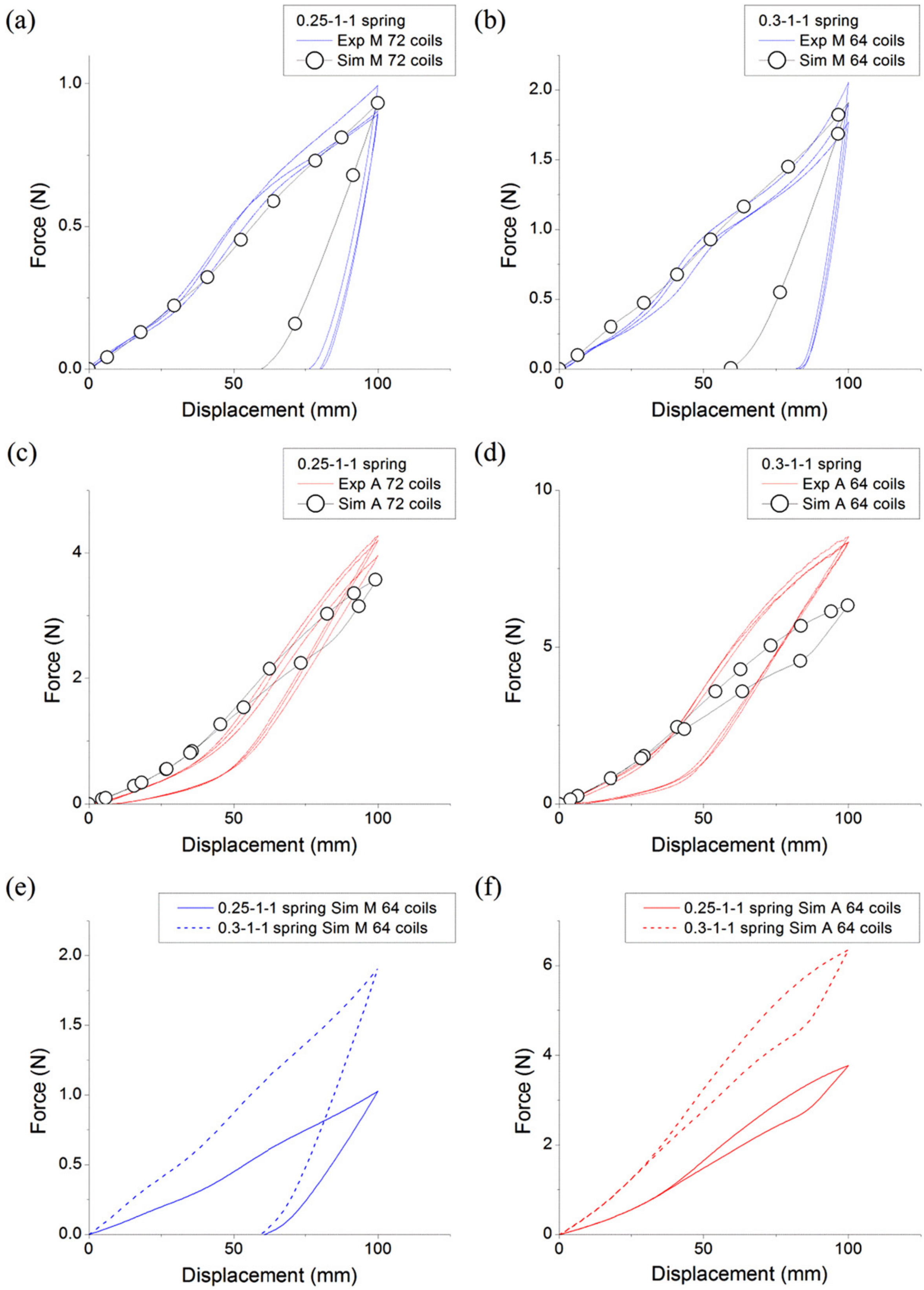

Figure 17. Displacement-to-force graphs of double-coil SMA springs with different wire diameters: (a) 0.25-1-1 spring at 20 °C, (b) 0.3-1-1 spring at 20 °C, (c) 0.25-1-1 spring at 200 °C, and (d) 0.3-1-1 spring at 200 °C. (e) and (f) are comparisons between the simulation results of 0.25-1-1 and 0.3-1-1 springs with same number of primary coils at 20 and 200 °C, respectively. Sim—simulation, Exp—experiment, M—martensite phase at 20 °C, and A—austenite phase at 200 °C. The coil number is the number of primary coils.

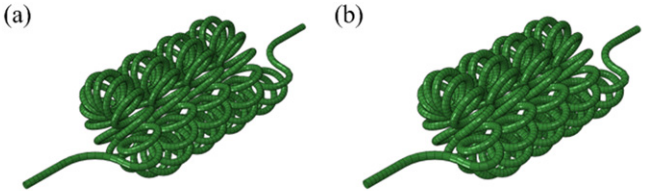

Figure 18. Simulation model of (a) 0.25-1-1 spring with 64 coils and (b) 0.3-1-1 spring with 64 coils.

4. Results and discussion

4.1. Effect of coil shape

Figure 11 shows the displacement-to-force profiles of the single- and double-coil SMA springs: one is the 0.25-1 spring, and the other is the 0.25-1-1 spring. The measured secondary coil diameter of the 0.25-1-1 spring is 1.18 mm. According to (2) and (3), the 0.25-1-1 spring can theoretically have a maximum of 63 primary coils under 4 secondary coils, but the actual 0.25-1-1 spring has 72 coils because of the increased secondary inner coil diameter. Hence, the two springs each have 72 primary coils (see figure 12).

As expected, the force profile of the double-coil SMA spring is different from that of the single-coil SMA spring. In the loading procedure at 20 °C, the force profile of the single-coil SMA spring shows one point of stiffness change at 20 mm (see figure 11(a)) while the force profile of the double-coil SMA spring shows two points of stiffness change at 40 and 60 mm (see figure 11(b)).

The change of stiffness of the double-coil SMA spring at the martensite phase is caused by two reasons: one is a geometrical transformation of the double-coil SMA spring from double-coil to single-coil and the other is a phase transformation of the double-coil SMA spring from the twinned martensite phase to the detwinned martensite phase. As can be seen in figure 13(a), the shape of the double-coil SMA spring changes from double coil to single coil until the displacement reaches 40 mm. For displacements lower than 40 mm, the distribution of the detwinned martensite volume fraction of the double-coil SMA spring is less than 0.2 (see figure 14), and the influence of the phase transformation from twinned martensite to detwinned martensite is not dominant to the change of stiffness . As a result, the deformation of less than 40 mm is only for the rigid-body motion and the stiffness of the double-coil SMA spring is for the double-coil configuration. When the displacement is more than 40 mm, the distribution of the detwinned martensite volume fraction increases but is still less than 0.4 until the displacement reaches 60 mm (see figure 14). The low detwinned martensite volume fraction means that the deformation between 40 and 60 mm is mainly affected by the rigid-body motion, as the deformation is less than 40 mm. Therefore, the stiffness in this range of deformation is determined by the single-coil configuration of the double-coil SMA spring actuator. When the displacement is more than 60 mm, the detwinned martensite volume fraction increases as the stress of the SMA spring increases (see figure 15), and the influence of the phase transformation from the twinned to detwinned martensite phase is considerably dominant to the change of stiffness. Therefore, the change of stiffness results from the interaction between the geometrical and phase transformation of the double-coil SMA spring.

In the austenite phase in figure 11(c), the force-to-displacement profile of a single-coil SMA spring shows a linear curve that indicates a constant stiffness. On the other hand, the profile of the double-coil SMA spring in figure 11(d) shows a nonlinear curve: the stiffness changes when the displacement goes above 40 mm. In figure 13(b), the configuration of the double-coil SMA spring transforms from a double coil to a single coil, and the configuration is similar to the single-coil shape at 40 mm displacement. This supports the slope change observed in the force profile during the austenite phase in figure 11(d), where the gentle slope of the double-coil SMA spring before 40 mm results from the double-coil configuration and the steep slope after 40 mm results from the single-coil configuration.

Table 6. Stiffness of 0.25-1-1 and 0.3-1-1 SMA springs in the martensite and austenite phases. Exp—experiment, Sim—Simulation, SD—Standard deviation, Error—percentage of difference between the experiment and simulation with respect to the simulation.

		Primary coil stiffness (N mm^{-1})							
		Martensite				Austenite			
Spring type	Number of primary coils	Sim	Exp	SD	Error(%)	Sim	Exp	SD	Error (%)
0.25-1-1	64	0.013	—	—	—	0.054	—	—	—
	72	0.012	0.014	0.0009	16.7	0.049	0.065	0.0024	32.7
0.3-1-1	64	0.022	0.028	0.0011	27.3	0.087	0.125	0.0077	43.7
		Secondary coil stiffness (N mm^{-1})							
		Martensite				Austenite			
Spring type	Number of primary coils	Sim	Exp	SD	Error(%)	Sim	Exp	SD	Error (%)
0.25-1-1	64	0.009	—	—	—	0.022	—	—	—
	72	0.008	0.008	0.0003	0	0.019	0.018	0.0008	−5.3
0.3-1-1	64	0.017	0.014	0.0009	−17.6	0.043	0.049	0.0006	14.0

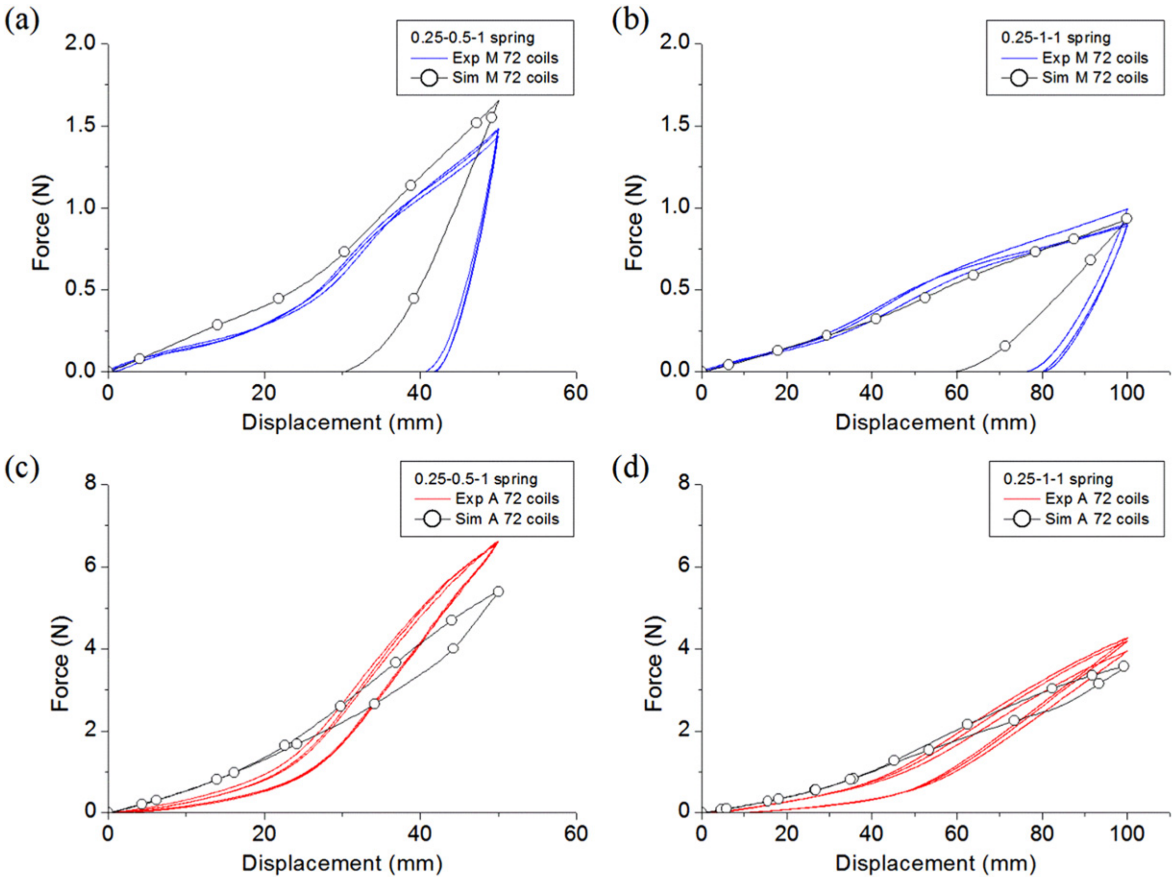

Figure 19. Displacement-to-force graphs of double-coil SMA springs with different primary inner coil diameters: (a) 0.25-0.5-1 spring at 20 °C, (b) 0.25-1-1 spring at 20 °C, (c) 0.25-0.5-1 spring at 200 °C, and (d) 0.25-1-1 spring at 200 °C. Sim—simulation, Exp—experiment, M—martensite phase at 20 °C, and A—austenite phase at 200 °C. The coil number is the number of primary coils.

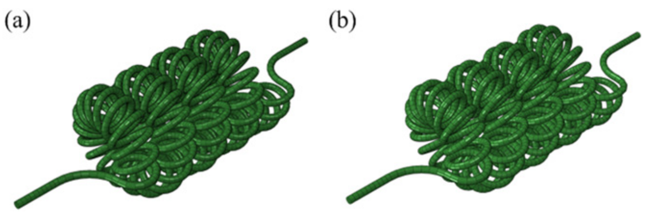

Figure 20. Simulation model of (a) 0.25-0.5-1 spring with 72 coils and (b) 0.25-1-1 spring with 72 coils.

The stiffnesses of the SMA springs are listed in table 5. The primary coil stiffnesses of the single- and double-coil SMA springs were obtained from the linear slope in the primary coil dominant region of the graph, as shown in figure 3(b). Similarly, the secondary coil stiffness of the double-coil SMA spring was obtained from the linear slope in the secondary coil dominant region. Owing to the double-coil configuration, the stiffness of the secondary coil dominant region of the 0.25-1-1 spring was quite low. However, the stiffness of the primary coil dominant region of the 0.25-1-1 spring was similar to that of the primary coil dominant region of the 0.25-1 spring because the geometry of the 0.25-1-1 spring changed from a double-coil shape to a single-coil shape; therefore, it can be regarded as a single-coil SMA spring.

According to the result of figure 11, the recovery ratio of the double-coil SMA spring is increased. The 0.25-1 spring has an initial length of 18.5 mm, and its maximum recoverable displacement is 80 mm; thus, the recovery ratio is approximately 432% (see figure 16(a)). The 0.25-1-1 spring has an initial length of 8 mm, and its maximum recoverable displacement is 100 mm; therefore, the recovery ratio is 1250% (see figure 16(b)).

4.2. Effect of wire diameter

Figure 17 shows the effect of the changing wire diameter of the double-coil SMA spring. The measured secondary inner coil diameter of the 0.25-1-1 spring is 1.18 mm and that of the 0.3-1-1 spring is 1.23 mm. According to (2) and (3), the 0.25-1-1 spring theoretically has 64 primary coils under 4 secondary coils, but has 72 coils in practice because of the increased secondary inner coil diameter. Likewise, the 0.3-1-1 spring theoretically has 55 primary coils under 4 secondary coils, but has 64 coils in practice.

As mentioned previously, the number of primary coils of the two double-coil SMA springs with different wire diameters should be matched to verify the effect of the wire diameter, but adjusting the number of primary coils per secondary coil is difficult in practice. Hence, we compare the simulation results of the 0.3-1-1 spring and the 0.25-1-1

Table 7. Stiffness of 0.25-0.5-1 and 0.25-1-1 SMA springs in the martensite and austenite phases. Exp—experiment, Sim—Simulation, SD—Standard deviation, Error—percentage of difference between the experiment and simulation with respect to the simulation.

		Primary coil stiffness (N mm^{-1})							
		Martensite				Austenite			
Spring type	Number of primary coils	Sim	Exp	SD	Error (%)	Sim	Exp	SD	Error (%)
0.25-0.5-1	72	0.048	0.05	0.0026	4.2	0.150	0.244	0.0057	62.7
0.25-1-1	72	0.012	0.014	0.0009	16.7	0.049	0.065	0.0024	32.7
		Secondary coil stiffness (N mm^{-1})							
		Martensite				Austenite			
Spring type	Number of primary coils	Sim	Exp	SD	Error (%)	Sim	Exp	SD	Error (%)
0.25-0.5-1	72	0.021	0.018	0.0008	−14.3	0.053	0.041	0.0031	−22.6
0.25-1-1	72	0.008	0.008	0.0003	0	0.019	0.018	0.0008	−5.3

spring with 64 coils. By doing so, we can observe that both springs have the same number of primary and secondary coils, and they have the same primary and secondary coil diameters except for the wire diameter (see figure 18). Therefore, it can be concluded that only the wire diameter affects the actuation characteristic in this group.

As shown in figure 17 and table 6, increasing the wire diameter increases the stiffness of both the primary and secondary coil dominant regions. The increment of the primary coil stiffness at the martensite and austenite phases are about 61 and 69%, and that of the secondary coil stiffness at the martensite and austenite phases are about 89 and 95%, respectively.

4.3. Effect of primary inner coil diameter

Figure 19 shows the effect of the primary inner coil diameter on the double-coil SMA spring. The measured secondary coil diameter of the 0.25-0.5-1 spring is 1.18 mm, which is the same as that of the 0.25-1-1 spring. Thus, both the 0.25-0.5-1 and 0.25-1-1 SMA springs have 72 primary coils and 4 secondary coils in practice (see figure 20).

As shown in figure 19 and table 7, changing the primary inner coil diameter affects the stiffness of both the primary and secondary coils. This result can be explained by considering a single-coil spring. Generally, the stiffness of a single-coil spring is inversely proportional to the cubic spring diameter. If the primary coil is considered a wire of a virtual single-coil spring and the secondary coil is considered a coil of the virtual single-coil spring, a double-coil spring can be regarded as a virtual single-coil spring. If the primary inner coil diameter increases while the other diameters are unchanged, the modulus of the virtual wire decreases so that the stiffness of the virtual single-coil spring also decreases. Therefore, increasing the primary inner coil diameter decreases not only the stiffness of the primary coil dominant region but also the stiffness of the secondary coil dominant region.

4.4. Effect of secondary inner coil diameter

Figure 21 shows the effect of the secondary inner coil diameter on the double-coil SMA spring. The measured secondary inner coil diameter of the 0.3-1-3 spring is 3.42 mm, and it has 156 primary coils and four secondary coils. The 0.3-1-3 spring can have a maximum of 139 coils theoretically but in practice has 156 coils because of the increased secondary inner coil diameter. In an approach similar to that in the simulation in the previous section 4.2, the number of primary coils of the 0.3-1-3 spring was matched with that of the 0.3-1-1 spring in the simulation to verify the effect of the changing secondary coil diameter. In the simulation, the 0.3-1-1 spring and the 0.3-1-3 spring had 64 primary coils and 4 secondary coils, and they were constructed with the same wire diameter and primary coil diameter (see figure 22). Hence, it can be concluded that only the secondary coil diameter affects the actuation characteristic of the double-coil SMA spring.

As shown in figure 21(e) and (f) and table 8, the simulation result of the 0.3-1-1 spring with 64 coils is compared with that of the 0.3-1-3 spring with 64 coils. The two springs have different stiffnesses in the secondary coil dominant region but have similar stiffnesses in the primary coil dominant region. This result can also be explained by employing the virtual single-coil spring as described in section 4.3. In the case of this parametric study group, the same spring index, which is the ratio of the spring diameter to the wire diameter, of the primary coil of the two double-coil SMA springs means that the moduli of the wires of the two virtual springs are the same. However, increasing the secondary coil diameter while maintaining the primary coil diameter increases the spring index of the virtual single-coil spring so that the stiffness of the virtual spring decreases. This works the same way in the double-coil spring. As a result, increasing the secondary coil diameter causes the stiffness of the secondary coil dominant region to decrease, whereas the stiffness of the primary coil dominant region remains stable.

4.5. Discussion

4.5.1. 4.5.1 Difference between the simulation and experiment. According to the force–displacement curves of the single- and double-coil SMA springs from section 4.1 to 4.4, there is some difference between the simulation and

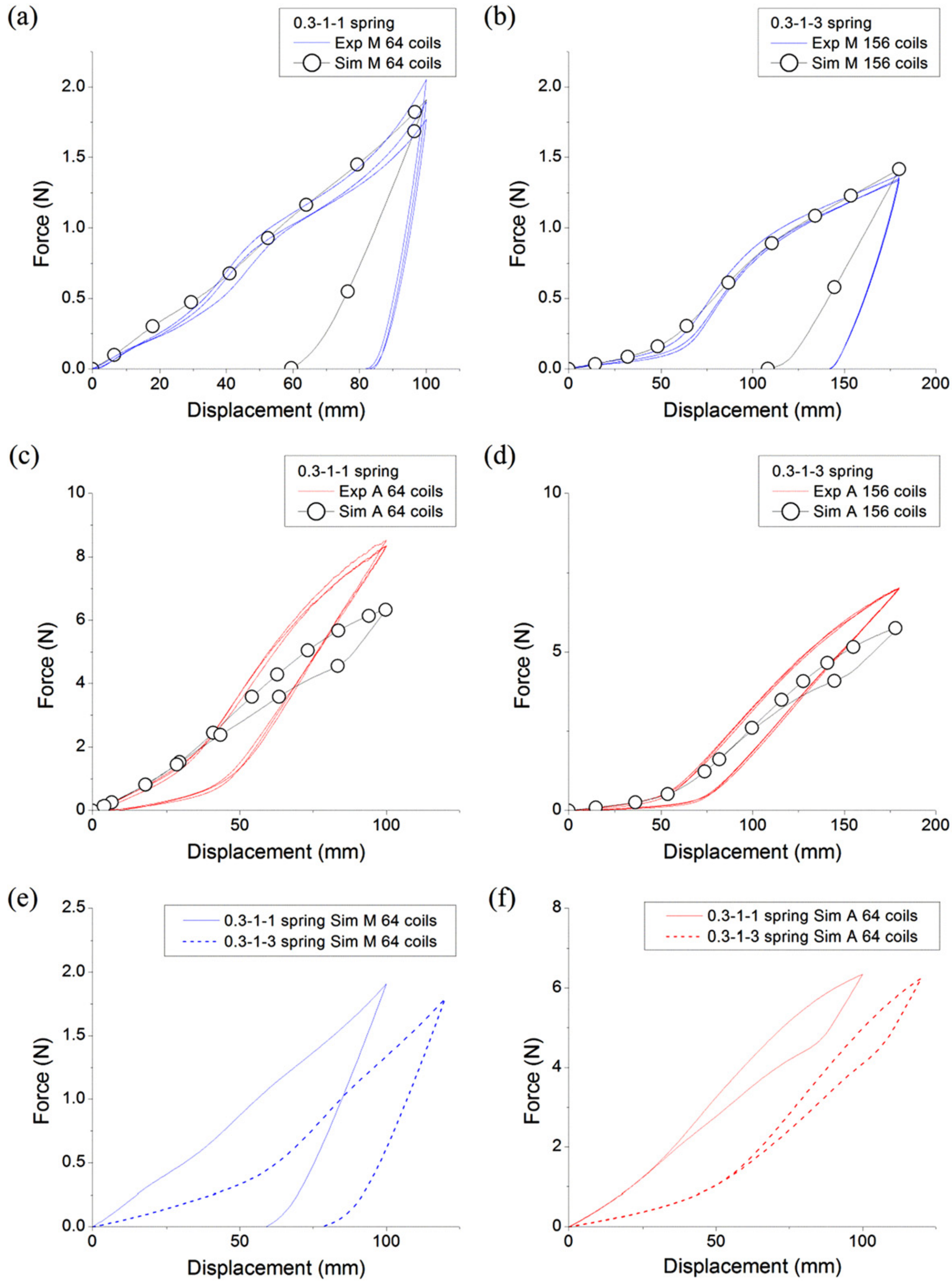

Figure 21. Displacement-to-force graphs of double-coil SMA springs with different secondary inner coil diameters: (a) 0.3-1-1 spring at 20 °C, (b) 0.3-1-3 spring at 20 °C, (c) 0.3-1-1 spring at 200 °C, and (d) 0.3-1-3 spring at 200 °C. (e) and (f) are comparisons between the simulation results of 0.3-1-1 and 0.3-1-3 springs with same number of primary coils at 20 and 200 °C, respectively. Sim—simulation, Exp—experiment, M—martensite phase at 20 °C, and A—austenite phase at 200 °C. The coil number is the number of primary coils.

experimental results. Firstly, the force–displacement curve of the single-coil SMA spring at low temperature obtained by simulation was higher than that obtained experimentally (see figure 10). The reason for this can be explained by the deviation of the estimated martensite finish temperature from that obtained through DSC. According to table 3 in section 3.2.1, the deviation of the estimated transformation temperatures (A^s, A^f, and M^s) is approximately ±1 °C. However, the deviation of the estimated martensite finish temperature (M^f) from the average value is ±5 °C because the

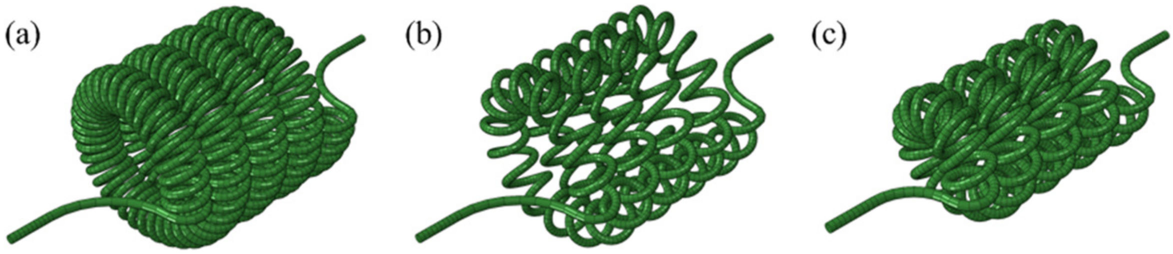

Figure 22. Simulation model of 0.3-1-3 spring with (a) 156 coils and (b) 64 coils and (c) 0.3-1-1 spring with 64 coils.

Table 8. Stiffnesses of 0.3-1-1 and 0.3-1-3 SMA springs in the martensite and austenite phases. Exp—experiment, Sim—Simulation, SD—Standard deviation, Error—percentage of difference between the experiment and simulation with respect to the simulation.

		Primary coil stiffness (N mm^{-1})							
		Martensite				Austenite			
Spring type	Number of primary coils	Sim	Exp	SD	Error (%)	Sim	Exp	SD	Error (%)
0.3-1-1	64	0.022	0.028	0.0011	27.3	0.087	0.125	0.0077	43.7
0.3-1-3	64	0.024	—	—	—	0.090	—	—	—
	156	0.014	0.018	0.0003	28.6	0.055	0.063	0.0003	14.5
		Secondary coil stiffness (N mm^{-1})							
		Martensite				Austenite			
Spring type	Number of primary coils	Sim	Exp	SD	Error (%)	Sim	Exp	SD	Error (%)
0.3-1-1	64	0.017	0.014	0.0009	−17.6	0.043	0.049	0.0006	14
0.3-1-3	64	0.006	—	—	—	0.017	—	—	—
	156	0.003	0.002	0.0005	−33.3	0.008	0.007	0.0013	−12.5

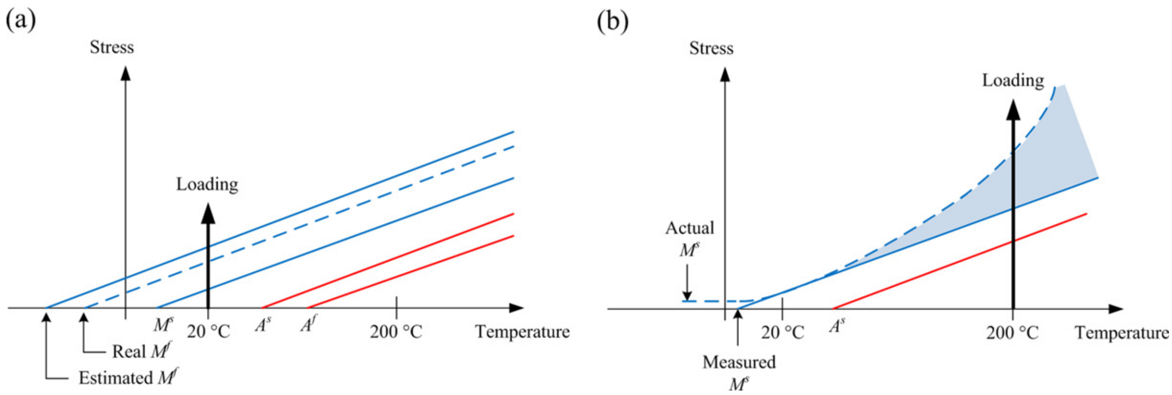

Figure 23. Stress–temperature diagram of SMA: (a) the effect of the change of martensite finish temperature and (b) the effect of the non-constant increase rate of martensite transformation start stress.

shape of the peak curve of the DSC in the martensite phase makes it difficult to determine M^f, as we mentioned in section 3.2.1. M^f is closely related to the maximum transformation stress in which the transformation finishes (i.e. from twinned martensite to detwinned martensite). For example, if the M^f is estimated to be a relatively lower value than the real value (see figure 23(a)), the analyzed force–displacement curve of the SMA spring is inevitably positioned higher than the force–deflection curve obtained experimentally. This fact explains why the analyzed force–displacement curve of the single-coil SMA spring is positioned higher than the experimentally obtained force–displacement curve at low temperature.

In figure 10, the stiffness of the single-coil SMA spring before the displacement of 30 mm at 200 °C in the simulation was almost same as in the experiment. However, the change of stiffness of the force-to-displacement profile in the simulation appeared at a displacement of 30 mm while the change of stiffness did not appear in experiment until the displacement reached 50 mm. This means that the forward phase transition from austenite to detwinned martensite occurred in the simulation whereas the phase transition did not occur in the experiment. Due to this, the results of the double-coil SMA springs showed that the stiffness of the primary coils of the double-coil SMA spring in the simulation was less than that in the experiment (see figures 11, 17, 19, and 21). The reason for this discrepancy in the force–displacement curve at high temperature is unclear, but it can be assumed that the material properties and the assumptions of the FEA model affect the results. First, as discussed previously, the estimated M^f had a large deviation compared to the other transformation temperatures, thus this could be one reason for the observed difference. Next, in FEA we used the Lagoudas model which assumes the increased rate of the transformation start stress is constant, like most SMA models. According to reference [32], however, the actual rate of transformation start stress increases monotonically as the temperature increases, as shown in figure 23(b). For this reason, the difference in transformation start stress between simulation and experiment increased as the temperature increased, although the difference was small at low temperature. The detailed match between the simulation and experiment results is out of the scope of this study, and will be progressed in future work.

4.5.2. Low load capacity. Although the recovery ratio of the double-coil SMA spring is large, the overall stiffness is reduced, and the secondary coil stiffness in particular is quite low. To use the full range of the shape recovery for actuation, the double-coil SMA spring should be stretched into a detwinned martensite phase by a sufficient external load. However, the external load to stretch this into a detwinned martensite phase is larger than the actuation force of the double-coil SMA spring in the secondary coil dominant region at the austenite phase. In this case, the actuator cannot return to its initial shrunk position. Therefore, conventional actuation methods for a single-coil SMA spring actuator, such as a constant loading actuation or an antagonistically connected actuation, are hard to use to generate the full range of shape recovery of the double-coil SMA spring actuator. To use the full shape recovery, the actuation of the double-coil SMA spring actuator should differ from conventional actuation methods. One way to do this is to only use a one-way shape transition without external loading. The double-coil SMA spring not only has a large longitudinal change but also has a considerable radial change. Thus, it can have a volumetric transformation from a fine wire to a bulky double-coil configuration which has a high surface area within a short length. Such kinds of geometrical changes would be useful in certain medical applications such as a filter with a high surface area within a short length for blood vessels or as a bulky scaffold to assist in the coagulation of blood, which can be used to fill an unnecessary hole in an organ. Another way to use full shape recovery is to vary the applied load along the shape transition of the double-coil SMA spring actuator, because the displacement-to-force profile of the double-coil SMA spring is nonlinear. In this case, the double-coil SMA spring can be used in a variable stiffness actuator.

5. Conclusion

We proposed a novel double-coil SMA spring actuator for a large actuation stroke with a compact size. The effect of the geometric parameters on the actuation characteristic of the double-coil SMA spring actuator was evaluated using a parametric study. For the parametric study, we categorized the SMA springs into four groups according to different geometric parameters and conducted a numerical FEA simulation and an experiment with a tensile test. To reflect the behavior of the SMA in FEA, the material properties of the SMA were obtained by the tensile test of the single-coil SMA spring actuator, and the Lagoudas model using these material properties was implemented in ABAQUS. The experimental results were compared with the numerical simulation results based on FEA; these were in good agreement with each other. The double-coil SMA spring actuator had an extremely large shape recovery ratio of approximately 1250% in comparison with the single-coil SMA spring actuator which had a shape recovery ratio of approximately 432% with the same geometric parameters. Furthermore, the displacement-to-force profile was changed to display nonlinear behavior due to the double-coiled configuration: the stiffness in the secondary coil dominant region was lower than that in the primary coil dominant region. The effect of the geometric parameters of the double-coil SMA spring is summarized as follows:

(i) The double-coiled geometry reduces the initial length of the SMA spring from a single-coil shape to a double-coil shape as expressed by the reduction ratio R

$$R = \frac{\pi \tan \alpha_1 \left(D_1 + d\right)\left(D_2 + d\right)}{d \tan \alpha_2 \left(D_2 + D_1 + 2d\right)}$$

where d, D_1, D_2, α_1, and α_2 are the wire diameter, primary inner coil diameter, secondary inner coil diameter, primary coil pitch angle, and secondary coil pitch angle, respectively.

(ii) Increasing the wire diameter increases the stiffness of both the primary and secondary coil dominant regions.

(iii) Increasing the primary inner coil diameter decreases the stiffness of both the primary coil dominant region and the secondary coil dominant region.

(iv) Increasing the secondary inner coil diameter decreases only the stiffness of the secondary coil dominant region.

The results of this study show that the double-coil SMA spring actuator has potential for a large actuation stroke despite the drawback of having a low load capacity. Further research should focus on developing analytical modeling and finding practical applications to use the characteristics of the double-coil SMA spring actuator.

Acknowledgments

This work was supported by the Priority Research Centers Program through the National Research Foundation of Korea (NRF) funded by the ministry of Education (2014048162), the National Research Foundation of Korea(NRF) grant funded by the Korea government(MEST) (2012R1A3A2048841), and a grant to the Bio-mimetic Robot Research Center funded by Defense Acquisition Program Administration (UD130070ID). In addition, the authors thank Sangeun Yoon at the Food Engineering Laboratory of Department of agricultural biotechnology in Seoul National University for advice and help in analysis of differential scanning calorimetry data.

References

[1] Otsuka K and Wayman C M 1999 *Shape Memory Materials* (Cambridge: Cambridge University Press) p 284
[2] Mohd Jani J *et al* 2014 A review of shape memory alloy research, applications and opportunities *Mater. Des.* **56** 1078–113
[3] Calkins F T and Mabe J H 2010 Shape memory alloy based morphing aerostructures *J. Mech. Des.* **132** 111012
[4] Sofla A Y N *et al* 2010 Shape morphing of aircraft wing: Status and challenges *Mater. Des.* **31** 1284–92
[5] Hutapea P *et al* 2008 Development of a smart wing *Aircr. Eng. Aerosp. Technol.* **80** 439–44
[6] Kode V R C and Cavusoglu M C 2007 Design and characterization of a novel hybrid actuator using shape memory alloy and dc micromotor for minimally invasive surgery applications *IEEE/ASME Trans. Mechatron.* **12** 455–64
[7] Duerig T, Pelton A and Stöckel D 1999 An overview of nitinol medical applications *Mater. Sci. Eng.* **273–275** 149–60
[8] Ho M *et al* 2012 Towards a meso-scale SMA-actuated MRI-compatible neurosurgical robot *IEEE Trans. Robot.* **28** 213–22
[9] Shi Z Y, Liu D and Wang T M 2014 A shape memory alloy-actuated surgical instrument with compact volume *Int. J. Med. Robot.* **10** 474–81
[10] Minkyun N *et al* 2012 Flea-inspired catapult mechanism for miniature jumping robots *IEEE Trans. Robot. Autom.* **28** 1007–18
[11] Gilardi G *et al* 2009 A shape memory alloy based tendon-driven actuation system for biomimetic artificial fingers, part II: modelling and control *Robotica* **28** 675–87
[12] Mazzolai B *et al* 2012 Soft-robotic arm inspired by the octopus: II. From artificial requirements to innovative technological solutions *Bioinspir. Biomim.* **7** 025005
[13] Koh J-S and Cho K-J 2013 Omega-shaped inchworm-inspired crawling robot with large-index-and-pitch (LIP) SMA spring actuators *IEEE/ASME Trans. Mechatron.* **18** 419–29
[14] Seok S *et al* 2013 Meshworm: a peristaltic soft robot with antagonistic nickel titanium coil actuators *IEEE/ASME Trans. Mechatron.* **18** 1485–97
[15] Hwang D and Higuchi T 2014 A cycloidal wobble motor driven by shape memory alloy wires *Smart Mater. Struct.* **23** 055023
[16] Leester-Schädel M *et al* 2008 Micro actuators on the basis of thin SMA foils *Microsyst. Technol.* **14** 697–704
[17] Ali M S *et al* 2014 Wireless displacement sensing of micromachined spiral-coil actuator using resonant frequency tracking *Sensors* **14** 12399–409
[18] Torres-Jara E *et al* 2010 Compliant modular shape memory alloy actuators *IEEE J. Robot. Autom.* **17** 78–87
[19] Paik J K, Hawkes E and Wood R J 2010 A novel low-profile shape memory alloy torsional actuator *Smart Mater. Struct.* **19** 125014
[20] An S-M *et al* 2012 Engineering design framework for a shape memory alloy coil spring actuator using a static two-state model *Smart Mater. Struct.* **21** 055009
[21] Shea H R *et al* 2014 Low spring index, large displacement shape memory alloy (SMA) coil actuators for use in macro- and micro-systems *Proc. SPIE* **8975** 897505
[22] Follador M *et al* 2012 A general method for the design and fabrication of shape memory alloy active spring actuators *Smart Mater. Struct.* **21** 115029
[23] Kaoua S A *et al* 2011 Numerical modelling of twin helical spring under tensile loading *Appl. Math. Modelling* **35** 1378–87
[24] Benghanem N *et al* 2007 Modelisation of thermoelastic linear behaviour of tungsten filaments in simple and twin helical spring configurations *Int. J. Solids Struct.* **44** 8159–76
[25] Grabitz R G *et al* 1998 Double-helix coil for occlusion of large patent ductus arteriosus: evaluation in a chronic Lamb model *J. Am. College Cardiol.* **31** 677–83
[26] Gilbert N and Allan 2014 Supercoiling in DNA and chromatin *Current Opinion in Genetics & Development* **25** 15–21
[27] Lee J-G *et al* 2012 The prediction of nonlinear behavior of double coil shape memory alloy spring *J. Comput. Struct. Eng. Inst. Korea* **25** 347–54
[28] Shaw J A, Churchill C B and Iadicola M A 2008 Tips and tricks for characterizing shape memory alloy wire: Part 1-differential scanning calorimetry and basic phenomena *Exp. Tech.* **32** 55–62
[29] Lagoudas D C, Bo Z and Qidwai M A 1996 A unified thermodynamic constitutive model for SMA and finite element analysis of active metal matrix composites *Mech. Compos. Mater. Struct.* **3** 153–79
[30] L'vov V A *et al* 2013 Entropy change of martensitic transformation in ferromagnetic shape memory alloys *Acta Mater.* **61** 1764–72
[31] Salzbrenner R J and Cohen M 1979 On the thermodynamics of thermoelastic martensitic transformations *Acta Metall.* **27** 739–48
[32] Shaw J A and Kyriakides S 1995 Thermomechanical aspects of NiTi *J. Mech. Phys. Solids* **43** 1243–81